Faculty of Engineering of University of Porto

Integrated Master's Degree in Bioengineering

Flow cytometry as a rapid tool to assess the microbial dynamics in anaerobic membrane bioreactors

---

Master Thesis Dissertation in Biological Engineering

Eduardo Machado Pinho

performed at

KAUST / Water Desalination and Reuse Centre

جامعة الملك عبدالله
للعلوم والتقنية

King Abdullah University of
Science and Technology

Supervisor at FEUP: **Dr Manuel Simões**
Supervisors at KAUST: **Dr Peiying Hong, Dr Hong Cheng**

September 2020

U.PORTO

FEUP FACULDADE DE ENGENHARIA
UNIVERSIDADE DO PORTO

© Eduardo Machado Pinho, 2020

Flow cytometry as a rapid tool to assess the microbial dynamics in anaerobic membrane bioreactors

Eduardo Machado Pinho
Integrated Master's Degree in Bioengineering

September 28, 2020

'Another beautiful day in quarantine!'

Pasi P. Paalanen

Preface

This thesis describes the results of a MSc internship research initiated in February 2020 and finished in August 2020 as part of the Integrated Master's Degree in Bioengineering at Faculty of Engineering of the University of Porto (FEUP). The work was performed at the Water Desalination and Reuse Centre (WDRC) of King Abdullah University of Science and Technology (KASUT).

This work intends to study the application of flow cytometry as a much faster and convenient alternative for analysing the complex microbial community present in anaerobic wastewater treatment. The simplicist approach used, consisting in the evaluation of only two main clusters, would favour the application of this tool for bioreactor process control.

I decided to choose that topic for my master thesis internship as I was motivated by the work developed at the WDRC in Dr Peiying Hong's group and I aimed in gaining more expertise in the operation of larger-scale bioreactor systems. Some of Dr Peiying Hong's research focuses on an exciting and highly interesting wastewater treatment technology, the anaerobic membrane bioreactors. Moreover, it was a unique and enthralling opportunity to work at a prestigious institution with a fascinating cultural context such as KAUST.

Due to the COVID-19 pandemic restrictions imposed by KAUST, from April onwards, no students were allowed to work in the labs. Thankfully and fortunately, due to Dr Peiying Hong's insistence, it was possible to keep the pilot reactor operating until the end of the commissioned period. Due to this, and also for the concern and for the patience during the writing phase, I am deeply thankful to Peiying. I also thank Jianqiang Zhou and Haleem Shah, respectively, for taking care of the bioreactor routine during quarantine period and running a portion of the flow cytometry samples, on my behalf.

To conclude, writing my thesis in year 2020 was challenging since I missed some of the experiments for which only practice would be the best teacher. Nevertheless, the main goals of my initial proposal have been accomplished and materialised in this work, contributing to a better knowledge associated with this topic.

Eduardo Pinho

Porto, September 2020

Resumo

Reatores anaeróbios de membrana (AnMBRs) têm vindo a ser usados como um meio bastante eficaz para tratar águas residuais municipais e, tal como qualquer outro tratamento biológico, o seu desempenho é inseparável do da comunidade microbiana. Os métodos mais usados para a avaliar são laboriosos, caros e lentos, e a citometria de fluxo (CF) tem emergido como uma alternativa mais rápida e conveniente capaz de elaborar "impressões digitais" microbianas. Desta forma, a CF poderá permitir uma maior racionalização do controlo e estabilidade do processo.

Nesta tese, um AnMBR piloto (50 L) foi operado por 146 dias a quatro tempos de retenção hidráulica (TRH): 24, 20, 16 e 12 horas. Os parâmetros avaliados caraterizaram o desempenho da operação do reator e da sua comunidade microbiológica. Para caraterizar o desempenho da operação, foram avaliados a produção de metano e a eficiência na remoção de matéria orgânica. O cálculo da produção de metano, baseou-se na composição do biogás, aferida por cromatografia gasosa, e o da eficiência, na concentração de matéria orgânica, aferida por espetrofotometria. As mudanças microbiológicas foram avaliadas por CF e os microrganismos divididos em grupos com alto e baixo conteúdo em ácidos nucleicos, HNA e LNA, respetivamente.

Os resultados indicam que o reator operado obteve melhor desempenho do que outros AnMBRs comparáveis. O mais bem-sucedido TRH foi o de 16 horas, onde o rendimento em metano e a remoção de matéria orgânica foram de 0.325 ± 0.008 $L.gCQO_{alimentado}^{-1}$ (82% do máximo teórico) e 98.8%±0.3%, respetivamente. A quantificação em HNA e LNA só foi possível para a biomassa suspensa e a ligada. Subpopulações dentro destes dois grupos correlacionaram-se com os parâmetros operacionais após adaptação a um novo TRH. O rácio HNA:LNA permitiu denotar a fase de estado estacionário de desempenho do reator para alguns dos TRHs.

Globalmente, verificou-se que a CF e a metodologia HNA/LNA têm elevado potencial na identificação de mudanças, ou mesmo de dinâmicas, microbiológicas, abrindo portas a uma abordagem mais simples e rápida para AnMBRs e para aferição da estabilidade do processo (rácio HNA:LNA). A sequenciação das mais relevantes (sub)populações microbianas ajudarão a verificar as conclusões postuladas e a traçar o perfil de "impressão digital" microbiológico do AnMBR.

Palavras-chave: Reatores anaeróbios de membrana, Citometria de fluxo, Dinâmicas de microrganismos anaeróbios, Tempo de retenção hidráulico.

Abstract

The anaerobic membrane bioreactor (AnMBR) is a highly efficient technology for the treatment of wastewaters of municipal origin and, as in any other biological treatment, its treatment performance is governed by the microbial consortia. The standard tools used to assess microbial performance are laborious, expensive and slow, and thus flow cytometry (FCM) has been emerging as a much faster and convenient alternative capable of establishing microbial fingerprinting profiles. Hence, FCM may be key to rationalise process control and stability.

In this thesis, a pilot AnMBR (50 L) was operated throughout 146 days at four hydraulic retention times (HRT): 24, 20, 16 and 12 hours. The assessed parameters characterised the performance of reactor operation and of its microbial community. To characterise the performance of operation, methane yield and organic matter removal efficiency were evaluated. The calculation of the methane yield was based on biogas composition, assessed using gas chromatography, and the concentration of organic matter, was measured by spectrophotometry. Microbial changes were assessed through FCM and the microorganisms clustered into groups with high and low nucleic acid content, HNA and LNA respectively.

The results showed that the operated reactor was better than any other comparable system. The most successful HRT time was the one of 16 h, with the highest methane yield and COD removal percentages, 0.325 ± 0.008 $L.gCOD_{feed}^{-1}$ (82% of the theoretical maximum) and 98.8%±0.3%, respectively. Quantification in HNA and LNA was only verified for suspended and attached biomass. Subpopulations within these two groups could be correlated with the operational parameters after adaptation to the induced HRT change. HNA to LNA ratio was positively linked with the steady-state performance of the bioreactor for some of the HRTs.

Globally, it was verified that FCM and HNA/LNA methodologies have great potential as tools to denote microbial changes, possibly even dynamics, paving the way towards a more simple and rapid analysis in AnMBRs and admeasurement of process stabilisation (HNA to LNA ratio). The sequencing of the most relevant microbial (sub)populations would help in verifying the postulated conclusions and in paving the way towards a microbial fingerprinting profile approach to AnMBRs.

Keywords: Anaerobic membrane bioreactors, Flow cytometry, Anaerobic microbial dynamics, Hydraulic retention time.

Acknowledgements

I would like to express my gratitude to Dr Peiying Hong for having welcomed me in her group at KAUST and also to Dr Hong Cheng for accepting me in his project. I am also thankful to my co-supervisor at FEUP, Dr Manuel Simões, for his feedback and support. Their advices helped me move forward with my research project.

I would also like to acknowledge the members of Dr Peiying Hong's group for the welcome upon my arrival and to Dr Luís Silva, from the Red Sea Research Centre, for all the help and knowledge regarding the flow cytometry!

I gratefully acknowledge the opportunity and financial support received from the Visiting Student Research Program (VSRP) from KAUST.

To all my friends that, despite any distances, throughout this year, immensely supported me (technical support as well), cheered me up and even heard my, sometimes, gibberish talking, thank you! To all the other new friends I made at KAUST, in particular to the Tuga group and to my roommates Pasi and Felipe, just watch-look: I would like to express my thanks for making my staying insanely remarkable!!

Ao amigo que quis embarcar nesta aventura comigo, por ter aceite esta ideia maluca, ter tido paciência para me aturar e não se importar de gastar uma fatia do ordenado em gelados, muito obrigado David!

À amiga que chegou a acreditar mais que eu nas minhas próprias capacidades, me motivou e ajudou mais que todos neste processo, e muitas vezes ao longo de toda esta caminhada na universidade, um muitíssimo obrigado, Margarida!

Por último, queria agradecer aos meus pais por acreditarem em mim e me possibilitarem tirar o curso e, em particular neste período de escrita, por cuidarem do meu bem-estar físico e moral. Fica à minha irmã um agradecimento especial por ser a minha maior fonte de motivação e inspiração!

Dedico este trabalho sobre bichinhos invisíveis às minhas avós que, felizmente, já não precisam mais de perguntar em que ano estou do curso!

Eduardo

Table of contents

List of figures

List of tables

Notation and glossary

$\%CH_4$	Methane percentage	
$\overline{\%CH_4}$	Average methane percentage	
$\bar{x}$	Average parcel	L or $L.d^{-1}$
COD	Chemical oxygen demand	$mg.L^{-1}$
F	Flow rate	$L.h^{-1}$
HRT	Hydraulic retention time	h
MLSS	Mixed liquor suspended solids	$g.L^{-1}$
OLR	Organic loading rate	$gCOD.L^{-1}.d^{-1}$
SRT	Solid retention time	d
t	Time	d
T	Temperature	^oC
TSS	Total suspended solids	$mg.L^{-1}$
V	Volume	L
Y	Yield	
x	Parcel	L or $L.d^{-1}$

Greek letters

Δ	Interval

Abbreviation list

AnMBR	Anaerobic membrane bioreactor
FCM	Flow cytometry
FITC	Fluorescein isothiocyanate
FL	Fluorescence
FSC	Forward scatter
HNA	High nucleic acid
LCFA	Long chain fatty acid
LNA	Low nucleic acid
PBS	Phosphate-buffered saline
PerCp	Peridinin-Chlorophyll-protein cyanine5.5
PMT	Photomultiplier tube
PVDF	Polyvinylidene difluoride
qPCR	Quantitative polymerase chain reaction
SSC	Sideward scatter
TCD	Thermal conductivity detector
TMP	Transmembrane pressure
UASB	Up-flow anaerobic sludge blanket
VFA	Volatile fatty acids

Chapter 1

Introduction

1.1. Problem statement

Wastewater is a natural consequence of human activity. It is a term generically applied to water that contains a "wide variety of contaminant agents, including plant nutrients and pathogenic microorganisms, metallic, and organic pollutants, but also microcontaminants" (Helmer et al., 1997). Amongst all types of wastewater, municipal wastewaters are the most abundant type and are characterized by low organic strength and high particulate organic matter content (Gouveia et al., 2015). The most traditional type of biological treatment applied to wastewaters of municipal origin is the aerobic activated sludge process, while anaerobic processes are more commonly employed in industrial settings for the treatment of industrial wastewater, characterised by higher organic strength (Chan et al., 2009; Liao et al., 2006). Amidst the anaerobic processes, anaerobic membrane bioreactors (AnMBRs), known from industrial applications, have already started being applied to municipal wastewaters. These reactors are quite aligned with the sustainable current mindset of employing technologies that produce clean water and clean energy as water scarcity, resources depletion and global warming are contemporary threats (Sikosana et al., 2019): they are cost-efficient (small footprint, no aeration costs and even production of profitable bioenergy (methane)), and they also produce an effluent of good quality enriched in nutrients, which may enable direct agricultural water reuse. The good effluent quality and high methane yields are justified by the decoupling of the hydraulic retention time from the solid's one through the use of the membrane. This decoupling enables the treatment of higher loads of wastewater while maintaining high biomass concentrations with the adequate time to get the microorganisms properly established (Berkessa et al., 2018; Chan et al., 2009; Harb & Hong, 2017).

Naturally, a key aspect of biological wastewater treatment is the microbial community. Anaerobic microorganisms, namely archaea and bacteria, work synergistically in a delicate balance in order to guarantee high and constant methane production, as well as the removal of organic matter (Gallert & Winter, 2005). By monitoring the microbial community, it becomes easier to understand the microbial dynamics and how they correlate with operational parameters, which is desirable as it might improve process quality and control. Among the monitoring techniques, molecular methods can be used to precisely quantify cells and gene copies, while omics-based

ones denote the functional and phylogenetic diversities in a non-targeted manner. However, their cost, speed and highly laborious setting limit their application (Perera et al., 2019; Zhang & Liu, 2019).

Flow cytometry (FCM) is one technique that has been emerging for being quick, cheap and convenient and, even though it is more commonly associated with the quantification of cells, correspondence of this data with phylogenetic one is possible. The capability of FCM to monitor cells population dynamics is known in the biotech field and is widely used for medical applications in both research and routine settings (Lambrecht et al., 2018). This technique can quantify discrete particles present on a sample based on their intrinsic (cell size, morphology, granularity and autofluorescence) and extrinsic (fluorescent stains) properties (Perera et al., 2019). The vast availability of dyes to target specific organelles, of lasers and filters to, respectively, excite and allow the detection of a particular target wavelength, and the possibility to sort and later sequence their genome can foster the knowledge on the microbial community of AnMBRs. The application of a nucleic acid fluorescent stain on samples enables the clustering of cell events with similar nucleic acids' properties. Koch et al. (2013) has proven the feasibility of this concept by tracing multiple clusters in wastewater samples and correlating them, through sorting and sequencing with phylogenetic data, elaborating a microbial barcode/microbial fingerprinting profile. Nevertheless, the analysis was centred in multiple subclusters which can make its application as a monitoring technique for AnMBRs impracticable due to their intrinsic microbial complexity. The two-clusters approach from Gasol & Morán (2015) would be a much more simpler way to monitor the microbial community. However, the simple qualification in high and low nuclei acid, HNA and LNA respectively, populations, couldn't yet be correlated with precise/unbiased phylogenetic data in order to start establishing the mentioned microbial fingerprinting profile.

1.2. Motivation

Prior to this moment and to the best of my knowledge, there were only few previous studies on the application of flow cytometry to pilot or full-scale AnMBRs with the purpose of establishing it as a tool to monitor their microbial populations.

Some authors have already proved that FCM could be applied for that aim. Gasol & Morán, (2015) and Wang et al. (2009) have applied a two-cluster strategy (LNA/HNA) without precisely characterising the populations, while Koch et al. (2013) and Lambrecht et al. (2018) used a multiple cluster-tracking strategy but with the establishment of a proper microbial fingerprinting profile. Nevertheless, (i) the diversity and stability of microbial populations, in particular of the bacterial populations, are different in AnMBRs (the mentioned studies were focused in natural communities, traditional wastewater treatment plants and/or anaerobic digesters) and may be altered with the change of scale (Regueiro et al., 2012), (ii) it was disregarded the change of operational parameters, namely the HRT, which strongly influences cell dynamics (iii) the studies did not look into the natural fluorescence of the archaeal microbial community and, most importantly, (iv) the ones for which a microbial fingerprinting profile has been developed were focused on tracking multiple microbial subclusters which hinders a fast and simple analysis and also adaptation of the method if any changes occur in the system.

2

In contrast with the previous mentioned studies that have not focused in AnMBRs of medium-large scale and have only established cytometric microbial fingerprinting profiles based on a complex cluster tracking strategy, this study aims at simplifying the tracking system with an HNA/LNA strategy for these types of reactors.

1.3. Project scope

The main goal of this dissertation, and hypothesis to be defended, is to prove that flow cytometry can be used as a rapid method to assess changes in the microbial community in anaerobic membrane bioreactors. The following objectives were designed and sorted to address the primary goal.

Firstly, to operate the pilot bioreactor and monitor its operational performance.

Secondly, to find the main microbial clusters and classify them by size, nuclear acid content and fluorescence intensity.

Thirdly, to correlate the main microbial clusters and any other sensitive subpopulations within them, with the changes in the operational parameters.

At last, to identify all the relevant (sub)populations in order to validate the conclusions from the previous goal and start establishing a microbial barcode/microbial fingerprinting profile for this system.

4

Chapter 2

Literature review

The following subsections are arranged in order to deliver the theoretical concepts related to the systems of the study, the anaerobic membrane bioreactor and its microbial community composition, and also related with the technique used for microbial analysis, the flow cytometry.

2.1. Anaerobic membrane bioreactors

Anaerobic membrane bioreactors (AnMBRs) are broadly defined as biological treatment processes operated without oxygen and using a membrane to provide complete solid-liquid separation (Liao et al., 2006). Both the anaerobic and membrane processes can have multiple possibilities (i.e. multiple designs and configurations).

The first proof of concept of AnMBRs appears to have been firstly reported in 1978, evolving from the knowledge on anaerobic treatment processes and aerobic membrane bioreactors. The module configuration of this first AnMBR was that of an external cross-flow membrane (requiring an extra pump). Later on, progresses on submerged aerobic MBRs led to the other module configuration, the submerged membrane, and, eventually it has also become possible to have the membrane submerged but in an external chamber. The early use of AnMBRs was to treat high organic strength wastewaters (e.g. the food industry). Nevertheless, it did not gain traction probably due to the high membrane costs and lack of understanding of the required micronutrients and operational parameters (temperature, pH, redox potentials) for methanogens' growth at that time (Dvořák et al., 2016; Faisal I. Hai, Kazuo Yamamoto, 2013; Jain, 2018).

The use of an anaerobic treatment and of a membrane have known advantages in the wastewater treatment field, namely and respectively, the limited sludge production and the decoupling of the hydraulic retention time from the solids one. In particular, the decoupling allows for more wastewater to be treated while maintaining a high biomass concentration with enough time to get the microorganisms properly established. Despite those known advantages, the recent interest on this technology arises mostly from (Faisal I. Hai, Kazuo Yamamoto, 2013; Ho & Sung, 2009; Jain, 2018):

- Advances in membrane technology. New materials and strategies for cleaning and fouling control;
- The promises for the sustainability. Biogas is produced and effluent is of good quality and enriched in nutrients, enabling water reuse;
- Cost. These types of bioreactors are more compact, do not require aeration and generate a profitable by-product (biogas/methane).

Nowadays, successful applications of these bioreactors can be found across multiple scales and even for low organic strength wastewaters (e.g. municipal wastewaters), proving their operational stability (i.e. good treatment efficiency with stable biogas production; Table 1).

As aforementioned, AnMBRs' main elements are the anaerobic treatment process and the membrane. As far as the former are concerned and is possible to observe in Table 1, the most commonly used reactor types are either the up-flow anaerobic sludge blanket (UASB) one or the continuous stirred-tank reactor (CSTR). CSTRs have been more traditionally employed as the use of stirrer can ensure a well-mixed flow regime which helps in the rate-limiting biological treatment steps. However, as effluent solids concentration of CSTRs is equal to the bulk solids concentration, heavy membrane fouling can be an obstacle. In UASB reactor applications, the suspension is due to the upward flow and gravity and the biological treatment. UASBs have proven to be useful in decreasing the suspended solids concentration being sent to the membrane as the sludge bed entraps most of the particulate matter by adsorption and biodegradation. In terms of membrane technology, there are multiple membrane configurations (flat sheet, hollow fibre, and tubular membranes), module configurations (external or submerged), materials (plastic, sintered steel, and ceramic) and modes of operation (under pressure or vacuum) available for AnMBRs (Table 1). There are problems that arise from the membrane use, the biggest hurdle being membrane fouling and design options should aim to mitigate it. In order to address some of these problems, a vast range of strategies have already been applied to AnMBRs and/or are current topics of research, namely strategies to control cake layer formation, membrane permeability and membrane cleaning (Faisal I. Hai, Kazuo Yamamoto, 2013; Shin & Bae, 2018).

Table 1. Multiple AnMBR systems used for wastewater treatment and their operational parameters. These systems were selected to have the highest similarity in temperature of operation, HRT time and OLR to the pilot reactor of this study. The first study presented includes results that can be found in Results and discussion section.

Type of wastewater	*Type of reactor*	*Configuration, scale and volume*	*Membrane characteristics*	*T [°C]*	*HRT [h]*	*SRT [d]*	*OLR [gCOD. $L^{-1}.d^{1}$]*	*Methane yield [$L.gCOD_{feed}^{-1}$]*	*% COD removal*	*References*
Synthetic	UASB	External, Pilot (36L)	PVDF, MF (pore size: 0.4 µm)	35	12 16 20 24	NA	1.21±0.05 1.53±0.03 2.00±0.07 2.58±0.05	0.20±0.02 0.29±0.02 0.325±0.08 0.321±0.09	91%±2% 94%±4% 98.9%±0.3% 99.1%±0.2%	This study
Maize-processing effluent	CSTR	External, Full-scale (2610000 L)	UF (pore size: <0.1 µm)	35	125	NA	2.9	NA	97%	Ross et al. (1992)
Municipal	UASB	External, Pilot (849 L)	PVDF, tubular UF (MWCO: 100 kDa)	22	6	180	NA	NA	93%	Herrera-Robledo et al. (2011)
Food processing and washing	CSTR	External, Pilot (400L)	PES, UF (MWCO: 20-70 kDa)	37	16-100	50	2.07±0.15	NA	73-94%	He et al. (2005)
Municipal	CSTR	Submerged, Pilot (350 L)	PES, UF (pore size: 38 nm)	35	19.2	680	0.5-1.1	0.27	<90%	Martinez-Sosa et al. (2011)
Diluted landfill leachate	CSTR	Submerged, bench-scale (29 L)	Polyamide, UF (pore size: 0.1 µm)	35	24	NA	0.7	0.25	<90%	Bohdziewicz et al. (2008)
Thermo-mechanical pulping pressate	UASB	Submerged, bench-scale (10 L)	PVDF, UF (MWCO: 70 kDa)	37	60	280	2.59±0.53	0.21±0.03	>95%	Gao et al. (2011)
Synthetic	UASB	External, bench-scale (4 L)	PVDF, MF (pore size: 0.3 µm)	35	44	1400	0.43	0.231	96.60%	Cheng et al. (2019)
Synthetic	UASB	External, bench-scale (2 L)	PVDF, MF (pore size: 0.3 µm)	35	22	700	0.86	0.220	96.20%	Cheng et al. (2019)
Synthetic	UASB	External, bench-scale (2 L)	PVDF, MF (pore size: 0.3 µm)	35	11	700	0.86	NA	>93%	Cheng & Hong (2017)
Synthetic	UASB	External, bench-scale (2 L)	PVDF, MF (pore size: 0.3 µm)	35	26	355	0.72	0.196	90-96%	Harb et al. (2015)
Synthetic	UASB	External, bench-scale (2 L)	PVDF, MF (pore size: 0.3 µm)	35	26	325	0.72	0.217	90-96%	Harb et al. (2015)

2.2. Anaerobic microbial metabolism

Anaerobic digestion is a fermentative process that uses organic matter present in the wastewater as a carbon source while generating biogas. Reactors operating under these conditions, such as the AnMBRs, are mostly governed by a biogas metabolic pathway (Figure 1), in which the microbial community works synergistically as in a balanced consortium to ensure the highest methane and COD removal yields from the fed wastewater.

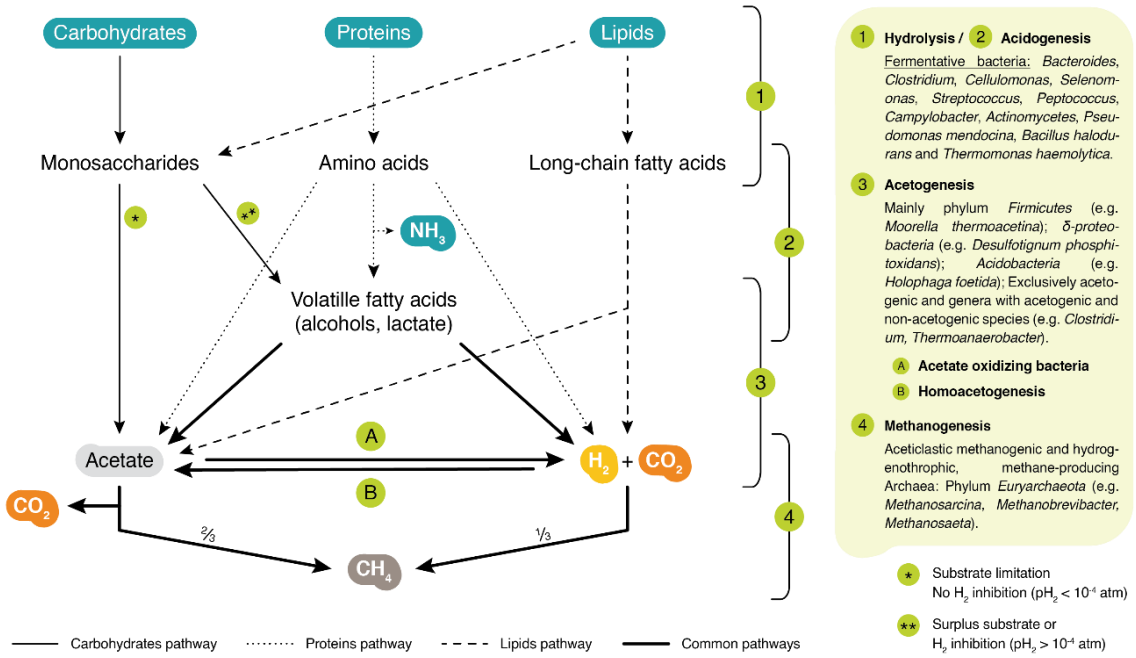

Figure 1. Simplified biogas metabolic pathways from complex polymers found in wastewater adapted from Gallert & Winter (2005) and Merlin Christy, Gopinath, & Divya (2014). Examples of microorganisms adapted from Korres et al. (2013).

Biogas production is divided into four main steps as depicted in Figure 1: (1) hydrolysis and (2) acidogenesis (fermentation), (3) acetogenesis and (4) methanogenesis, according to Ali Shah et al. (2014), Gallert & Winter (2005) and Lier et al. (2008):

(1) Hydrolysis

As the main biopolymers in sewage are proteins, carbohydrates, and lipids, hydrolysis (Figure 1 (1)) is employed in their surface by obligate or facultative anaerobes by secreted exo-enzymes. The resulting products are smaller molecules that can penetrate the cell barrier. If the substrates are complex, as the free accessible surface area is reduced, this step can be rate-limiting.

(2) Acidogenesis

Inside the cells, amino acids and simple sugars, products from the previous step, are fermented or anaerobically oxidised mainly into volatile fatty acids (VFAs) and carbonic acid (Figure 1 (2)), thus the name acidogenesis. Many of the microorganisms from this step are also hydrolytic, and thus hydrolysis and acidogenesis are sometimes also referred to as fermentation step. Acidogenesis is the fastest conversion step of all but, due to the souring effect of this step, either the medium needs to have some buffering capacity, or the subsequent microorganisms must metabolise the resulting acids at a sufficiently high rate to prevent the detrimental effect on their activity.

(3) Acetogenesis

The VFAs and other products of the previous step, other than acetate, are further converted to acetate, hydrogen gas, and carbon dioxide (Figure 1 (3)) by the acetogenic bacteria. Long chain fatty acids (LCFAs) are converted by specific acetogenic bacteria directly to H_2 and CO_2 (Figure 1 (3)). Although these bacteria are obligate hydrogen producers, they are also inhibited by hydrogen, thus requiring the help from methanogens and sulphate-reducing bacteria to control H_2 levels. Homoacetogenesis is a sub-step of acidogenesis that consists of the formation of acetate from H_2 and CO_2 (Figure 1 (3B)). Contrarily, acetate oxidizing bacteria can do the reverse (Figure 1 (3A)).

(4) Methanogenesis

The last step is the methane formation either from acetate (approximately two-thirds of the total) or from H_2 and CO_2. The growth rate of the microorganisms that consume acetate, the acetoclastic methanogens, is slow (several days or even more), accounting for one of the main reasons for the long start-up times of AnMBRs. The most common methanogens of this type in anaerobic high COD rate systems with high SRTs are *Methanosaeta spp.* and their dominance is linked with the reactor's steady-state and effective wastewater treatment (very low COD, particularly acetate). Those that produce methane from H_2 and CO_2 are the hydrogenotrophic methanogens with much shorter doubling times (4-12 h). Most of the *Methanosarcina spp.* are of this type and surpass others in growth rate for high COD concentrations (> 25 mgCOD.L^{-1}). The methanogenic microorganisms are considered, amongst all, the slowest growth consortia and the most vulnerable of all to environmental changes (Jain, 2018).

Other anaerobic microbial processes involved in wastewater treatment, such as denitrification, do not occur, unless the influent contains nitrate (NO_3^-) and the correspondent microorganisms (the denitrifying microorganisms, also present in the consortia) are unable to use oxygen as an electron acceptor. Nonetheless, under anoxic conditions, the denitrifying microorganisms are not the only ones to change their preferences. Sulphate (SO_4^{2-}) or sulphite (SO_3^{2-}) and iron (Fe^{3+}) may also be used as electron acceptors by specific bacteria like, sulphate reducers that can opt between all of the above inorganic species. These microorganisms compete with the methanogens under the absolute lack of O_2 (Lier et al., 2008).

As far as denitrification is concerned, the preliminary, essential, and also possible stand-alone step in the use of this N-source is nitrate reduction to nitrite (NO_2^-) (e.g. for glucose, Equation 1). There are actually more microorganisms able to perform this step rather than to transform the nitrite afterwards (Lam & Kuypers, 2011).

$$NO_3^- + {}^1/_{12}\, C_5H_{12}O_6 \rightarrow NO_2^- + {}^1/_2\, CO_2 + {}^1/_2\, H_2O \qquad \text{Equation 1}$$

As under anaerobic conditions, nitrate reduction is a dissimilatory process, two types of reaction may occur subsequently:

A) Reduction of nitrite to gaseous nitrogen or nitrous oxide (Equation 2).

$$NO_2^- + {}^1/_8\, C_5H_{12}O_6 + H_2O \rightarrow {}^1/_2\, N_2 + {}^3/_4\, CO_2 + {}^5/_4\, H_2O + OH^- \qquad \text{Equation 2}$$

B) Ammonification, via nitrite – Dissimilatory nitrate reduction to ammonium, DNRA.

The process is mediated by the enzyme cytochrome c nitrite reductase, which can also reduce nitric oxide to ammonia (Lam & Kuypers, 2011). Moreover, ammonia is a consequence of protein digestion and thus, high ammonia concentrations are commonly found in treated effluents by anaerobic processes (Akunna et al., 1992).

According to Cheng et al. (2019) and Win et al. (2016), some of the microorganisms present in the AnMBR system, and to which information regarding nucleotide number was found, are the ones present in Table 2.

Table 2. Example of microbial species presented in AnMBRs. The number of nucleotides was consulted at KEGG database.

	Phylogenetic affiliation	***Remark***	***No. nucleotides***
Fermentative bacteria	*Sulfurovum sp.*	Hydrolysis	2562277
	Shewanella irciniae	Acidogenesis	4545906
	Lactococcus		2365589
	Paludibacter	Acidogenesis	3685504
	Petrimonas		3693233
	Alteromonas sp.	Hydrolysis	4480937
	Enterobacter sp.	Acidogenesis	4676461
Acetogenic	*Acetoanaerobium*		2715461
	Desulfovibrio	Sulphate-reducing bacteria	3730232
	Geobacter	Sulphate-reducing bacteria	3814128
	Clostridium sp.		4132880
	Citrobacter sp.	Also acidogen	4735357
Syntrophs *	*Syntrophomonas*		2936195
Methanogens	*Methanobacterium sp.*	Hydrogenotrophic	2029766
	Methanocella paludicola	Hydrogenotrophic	2957635
	Methanothermus fervidus	Hydrogenotrophic	1243342
	Methanotorris igenus	Hydrogenotrophic	1854197
	Methanospirillum	Hydrogenotrophic	3544738
	Methanosaeta	Acetoclastic	2571034
	Methanosarcina acetivarans	Acetoclastic	5751492

***** Hydrogen-consuming organisms, may include methanogens, sulphate-reducers, and acetogens.

The above microorganisms are representative of the biogas production steps previously mentioned, but there are plenty more microorganisms present in a wastewater treatment anaerobic bioreactor. Most of all, regarding microorganisms, it is important to consider that this synergetic relationship is built and maintained to achieve an optimal wastewater treatment, and that it is based on a delicate equilibrium between the microbial populations inside an anaerobic membrane bioreactor. Hence, operational parameters such as the hydraulic retention times (HRT) can highly impact the type of community that will be created and sustained and consequently, treatment quality and biogas production. In theory, the lower the HRT time, the higher the

volumes of wastewater that can be treated per day, and the higher, the organic loading rates, consequently. If the microorganisms can bear this augmented hydraulic stress, then the potential methane production is greater. However, decreasing the HRT too much may also lead to the accumulation of volatile fatty acids, inhibiting methanogenesis, and thus, reducing methane yield (Win et al., 2016). According to the same author, regardless the HRT variation, methanogenic microorganisms such as *Methanosaeta*, *Methanobacterium*, *Methanotorris*, *Methanothermus*, and *Methanosarcina* are dominant populations with respect to the total microbial community. In experiments in which the hydraulic shock has been a subject, it has been reported that after a shock loading period, the microbial community exhibited significant changes, even within the ranks of methanogens (Vincent et al., 2018). Such change can also be due to competition with bacteria, such as the homoacetogenic, that can have a preferential and faster growth under those augmented stress conditions (Win et al., 2016).

2.3. Monitoring techniques

2.3.1. Overview

The identification of the microorganisms present in wastewater treatment and the study of their interactions can be useful for developing more sophisticated process control strategies. In Table 3, there is a summary of the available techniques used to characterise microorganisms and microbial dynamics.

Table 3. Summary of methods used to measure the density, structure and composition, and activities of the microbial community (Zhang & Liu, 2019).

MICROBIAL DENSITY	Cultivation methods → HPC and selective/differential media
	Cell counting → Microscopic counts, Flow cytometry
	Molecular methods → qPCR, viable qPCR, ddPCR
COMMUNITY STRUCTURE AND COMPOSITION	Community fingerprinting → DGGE, T-RFLP, PCR-ALH, SSCP
	16S rRNA gene amplicon → Sanger sequencing, NGS
	16S rRNA gene hybridization → DNA microarray
	Spatial distribution → FISH, SEM
MICROBIAL ACTIVITIES	Adenosine triphosphate (ATP) assay
	Enzymatic activity tests
	Assimilable organic carbon (AOC) assay

HPC, heterotrophic plate count; qPCR, quantitative polymerase chain reaction (PCR); ddPCR, digital droplet PCR; DGGE, denaturing gradient gel electrophoresis; T-RFLP, terminal restriction fragment length polymorphism; PCR-ALH: amplicon length heterogeneity; SSCP, single strand conformation polymorphism; NGS, next-generation sequencing; FISH, fluorescence in-situ hybridization; SEM, scanning electron microscopy;

Among the above techniques, many are mostly only used in research settings, and microbial activities, in particular, are not under the scope of this work. In terms of microbial density tools, cultivation methods, despite being the most conventional monitoring tool, are not considered robust and reliable nowadays (Wang et al., 2010; Zhang & Liu, 2019). Furthermore, the molecular methods, such as the qPCR, have the problem of being primer dependent , even though an advantage of them is their specificity allowing precise quantification of targeted gene copies that can be converted in cell numbers (Koch et al., 2013). As far as techniques that denote interactions of the microbial consortia are concerned, omics-based ones (e.g. metagenomics, a DNA-based technique) are remarkable, denoting the functional and phylogenetic diversities in a non-targeted manner. Nevertheless, the cost, speed and non-existence of well-curated databases may limit their application (Perera et al., 2019; Zhang & Liu, 2019). Alternatively, flow cytometry (FCM) is one technique more often associated with microbial density and that does not give, at least at a first glance, any information on the phylogenetic relations. Yet, as it is possible to correlate FCM data with phylogenetic information and FCM is a very quick, cheap and convenient technique, it has been emerging as a very promising approach as a wastewater monitoring tool (Hammes & Egli, 2010; Koch et al., 2013; Lambrecht et al., 2018; Perera et al., 2019; Safford & Bischel, 2019; Wang et al., 2010).

2.3.2. Flow cytometry

Flow cytometry refers to the broad suite of techniques that include the measurement of several properties of particles travelling in a pressurized flow in front of a light source (Gasol & Morán, 2015). Flow cytometers are used to measure not only cells, but also viruses, nuclei, chromosomes, DNA fragments and latex beads, thus term “particle”.

The first approach towards what one can mostly link to a flow cytometer nowadays is generally acknowledged to Andrew Moldavan in 1934 and was developed to count red blood cells and neutral-red-stained yeast cells. In a microscope, cells were forced through a capillary tube placed on the microscope stage, being individually illuminated while flowing in a single file. Any signals coming from the cells were registered by a photodetector attached to the microscope eyepiece. Later in 1953, Wallace H. Coulter has patented the first impedance-based cytometer. At last, throughout the 60s and beginning of the 70s, work by Fulwyler, Dittrich, Göhde, Van Dilla, Herzenberg and Bonner led to significant changes in the over-all design, the optimisation of the device to be fluorescence-based and the sorting. Sorting, in the form of what is called fluorescence-activated cell sorting (FACS), enabled the separation of particles from the sample based on their specific fluorescence characteristics and light-scattering properties, and consequently promoted downstream visualization, molecular or functional analyses (Givan, 2001; Hawley & Hawley, 2011).

In Figure 2, it is represented the FCM approach without the sorting component.

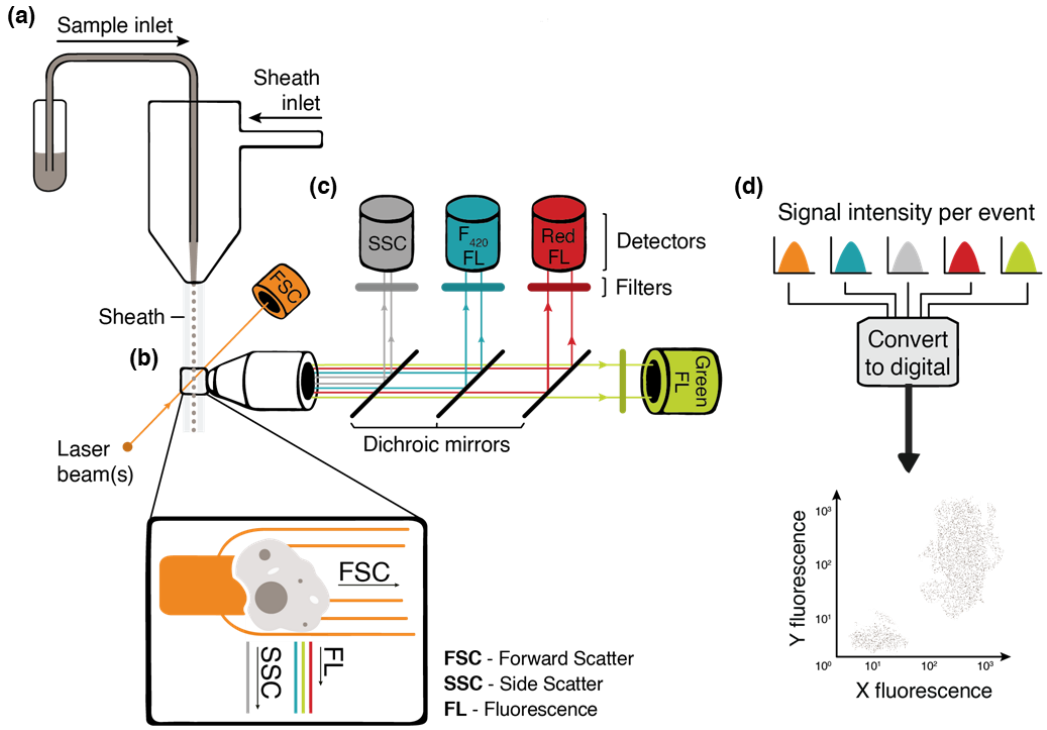

Figure 2. Principle of flow cytometry, (a) the suspension of particles is mixed with the sheath fluid that will carry and align the particles so that they pass through a narrow channel and into the laser intercept, (b) the stream of particles passes in front of laser beams (defined wavelength) and an objective lens collects light emitted by the particles (see zoomed details). If the FCM is equipped with more than one laser, each will act at different spots along the flow stream, (c) an appropriate system of lens and filters allow detectors to measure specific wavelength signals emitted by cells, (d) computers correlate the signals that were stored in data files. Adapted from Boster Biological Technology (n.d.) and Scintillon Institute (n.d.).

The device starts by aspirating the sample at an adequate flow rate and then mixing it with the sheath fluid, these measures should ensure that cells are aligned and well separated (Figure 2a). When beamed by one of the lasers, particles will refract some of the light in the forward direction (information collected by the forward scatter (FSC)) and scatter some other, which can also be perceived as emited fluorescence (Figure 2b). The scattered light is a reflex of their internal complexity or morphology (detected in the sideward scatter (SSC)). The emitted fluorescence may be either due to natural background (auto-) fluorescence or excitable components of the particle. In most cases, particles have been stained with dyes or specific probes that have compounds that can be excited by the beamed light wavelength (i.e. its maximum absorption wavelength spectra matches the beamed wavelength) and emit light in a different wavelength due to the deexcitation of such compounds. The fluorescent dyes/probes can be non-specific for a structure or as specific as antibody link. Alternatively, the dye itself may fluoresce when it is bound to a cellular component. The detectors will gather the light from each of the "events" (Figure 2c). There are the photodiodes that collect the information related with size (FSC information), being positioned head-on along the direction of the laser beam and. In addition, and for the remaining scattered light, the photodetectors used are photomultiplier tubes (PMT) which detect light of different wavelengths thanks to appropriate filters. Such filters are mainly bandpass, defining a range of wavelengths that are allowed to pass to the PMT or long pass, enabling light from inferior wavelength to pass to the detector. At last, the detected signal intensities read by each detetector are converted to digital. Each event will be turned into a vector with data regarding each of the signals that have been assessed, and, with this information, plots can be drawn (Figure 2d). In the plots, the preferrential agregation regions, the clusters, can be

later explored by encaging such groups in drawn "gates", i.e. looking at their behaviour in different axis to look for similarities.

The great advantages of FCM arise from (i) ease in analysing, (ii) robustness, (iii) huge potential for automation, (iv) adaptable to different types of samples and methods, (v) rapid analysis of large amount of cells (500 to more than 5000 events per second), (vi) the variety in the light sources that can be used to illuminate them, and the (vii) detectors that can record information on the particle-scattered light plus (viii) the fluorescence emitted either by natural pigments or fluorescent probes. With this technique, the individual characteristics of a large number of cells can be enumerated, correlated, and summarized (Gasol & Morán, 2015; Hammes & Egli, 2010).

Despite the vast application within the medical field (Cossarizza et al., 2019; Lambrecht et al., 2018), FCM can provide a wealth of information regarding the microbial characteristics of water samples (Hammes & Egli, 2010).

Flow cytometry, through staining and sorting, can be used to cluster microbial communities that share similar characteristics. Moreover, non-cell particles can be easily gated out of the analysis as scatter and fluorescence data denote a big array of cellular characteristics such as relative size, complexity, cell viability and nucleic-acid content. Hence, the mentioned communities can be identified and it can be established a unique cytometric "fingerprint" of the microbial community present in a water sample, helping scientists in recognising keystone microbial species and subpopulations crucial to particular wastewater treatment processes (Koch et al., 2014).

The identification and tracking of microbial subpopulations based on clusters of cell subpopulations with similar DNA abundance applied to wastewater treatment is not new and has been extensively studied by Koch et al. (2013). The published work proved that FCM could be used for that aim but the analysis was centred in multiple subclusters which can make its application to wastewater samples impracticable due to their intrinsic microbial complexity (Figure 3a).

Other bacterial groups can be distinguished using FCM. There are at least two main ubiquitous ones, ultimately labelled as high and low nucleic acid bacteria, respectively, HNA and LNA (Figure 3b), that could only be set apart with the use of specific nucleic acid stains (among which SYBR Green I®; Bouvier et al., 2007).

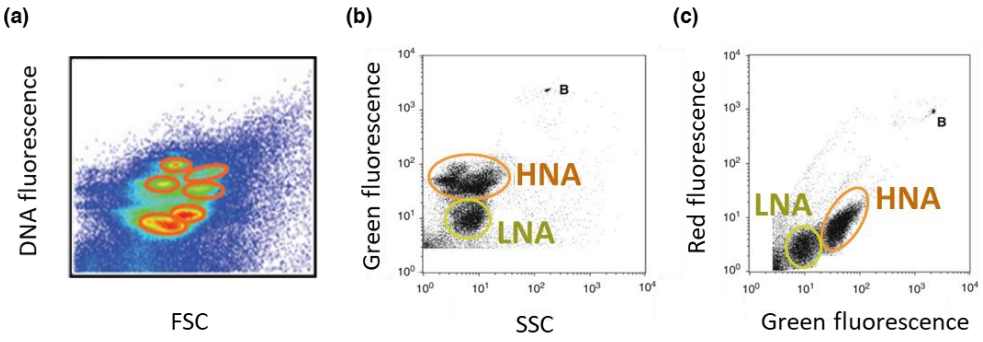

Figure 3. Clustering approaches with flow cytometry, (a) Koch et al. (2013) multiple cluster approach based on the size (forward scatter, FSC) and nucleic acid fluorescence from DAPI® (DNA fluorescence detected with a 450±32.5 nm optic filter) on a biogas production CSTR reactor, and (b-c) Gasol & Morán (2015) two-cluster approach, the high and low nucleic acid bacteria, respectively, HNA and LNA in marine samples based on (b) the morphology (side scatter, SSC, that also carries size information) and the nucleic acid fluorescence from SYBR GREEN I® (green fluorescence detected with a 530±15 nm optic filter), and (c) the nucleic acid content (green fluorescence) and the natural red fluorescence.

This division of microbial subpopulations in only two groups based on total nucleic acid staining is one of the most interesting, yet controversial, outcomes of the use of FCM, as this technique is the only method that clearly defines only those two clusters (Hammes & Egli, 2010). HNA/LNA distinction is possible for all aquatic samples, including wastewater and largely applied in fresh water ecosystems (Gasol & Morán, 2015; Proctor et al., 2018). Nevertheless, the role and composition of these bacterial groups are not defined, and some studies even suggest some mobility between them (Bouvier et al., 2007). Some bacterial communities are intrinsic to each of the groups, but the existence of the others that can be present in both clusters (i.e. that have mobility) has even generated a debate whether LNA could symbolise either an inactive fraction of the same specie (recently disregarded) or a viable but non-culturable fraction of it (Bouvier et al., 2007; Hammes & Egli, 2010). As far as the intrinsic groups are concerned, those may be positively linked with either larger genome sizes or by exhibiting higher metabolic activity (also detectable through mRNA) but not to viability (Wang et al., 2009). LNA population has been correlated positively with small genome size and metabolic dependencies on other microorganisms (Proctor et al., 2018) and HNA population, with heterotrophic productivity (Belzile et al., 2008).

In the very particular context of methanogenic archaea, Lambrecht et al. (2017) have documented and organised an FCM approach based on the excitement of the cofactor F_{420}. Upon being oxidised through covalent binding of the second and third hydrogen atom in methanogenesis ($CH–CH_2–CH_3$) (Figure 4a), this cofactor emits fluorescence if excited at around 420 nm (Figure 4b).

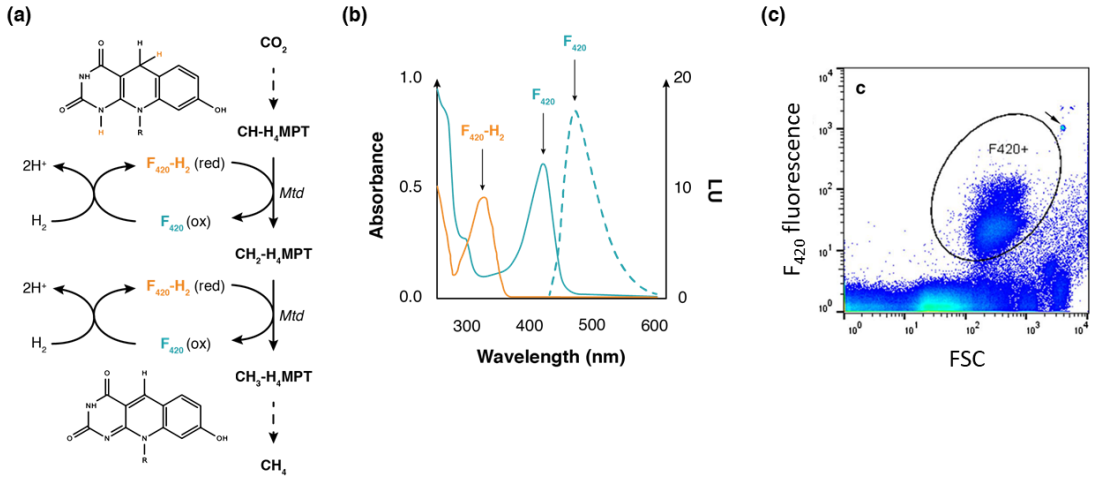

Figure 4. Coenzyme F_{420} properties, (a) F_{420} oxidation during carbon assembly (MPT – Methanopterin; Mtd – F_{420}-reducing methylene-H4 MPT dehydrogenase), (b) Spectrophotometric identification of reduced and oxidised F_{420} (continuous line denotes absorbance and dotted line, fluorescence emission) with maximum absorbance of the oxidised state at 420 nm and emission at 470-480 nm adapted from Bashiri et al. (2018) and Greening et al. (2016), (c) flow cytometry detection of cells expressing oxidised F_{420} (gate F_{420}+) (the arrow marks the control beads) adapted from Lambrecht et al. (2017).

According to the author, in a non-stained sample, it should be possible to detect higher fluorescence intensity in an appropriate detector-filter system for the cofactor F_{420} emission (Figure 4c). The detached group in Figure 4c has been proven by this author (Lambrecht et al., 2017) to be the methanogenic archaea.

Therefore, the HNA and LNA quantification seems like a much more simple and direct approach than tracking multiple subclusters, which can easily change in such a complex microbial environment as the wastewater one is. As these two populations could be used to denote changes, by identifying any intrinsic bacterial subpopulations within these groups, a microbial fingerprinting profile could be established. This profile could ultimately lead to the development of an HNA/LNA-based robust strategy for system control possible to be applied to wastewater treatment reactors.

Chapter 3

Methods

The following subsections address the goals highlighted in the Project scope subsection.

As far as the first goal (pilot reactor operation and performance monitoring) is concerned, the pilot bioreactor has been operated at four different HRTs, aiming to make this reactor treat competitive volumes of influent per day. The operational parameters monitored were the methane yield and the organic matter removal efficiency.

To address the second and third goals into finding, classifying and monitoring the main microbial clusters, as well as subpopulations, flow cytometry has been used.

The fourth goal (sorting and sequencing of relevant (sub)populations) could not be done due to time limitations.

3.1. Pilot bioreactor

3.1.1. Operation

The experiments were carried in a pilot AnMBR reactor (Figure 5a) composed of two parts: an up flow anaerobic sludge blanket (UASB) reactor, the sludge tank and an external compartment tank with an immersed membrane, the membrane tank. The total volume of each of the tanks was 50 L being the effective volume 36 L. The temperature was maintained at 35 °C (mesophilic conditions), the headspace pressure at 0 KPa and the pH of the sludge tank was set at 7 in an automatic control module. The membrane tank had a submerged cross-flow flat sheet polyvinylidene difluoride (PVDF) microfiltration membrane (nominal pore size of 0.4 µm; PHILOS membrane, Korea). Throughout all bioreactor operation, the membrane was not cleaned or changed, but the pressure was monitored not to exceed 40 kPa for means of transmembrane pressure (TMP) control. The peristaltic Longer Pumps® YZ1515x (Longer Precision Pump Co., Ltd, Hebei, China) in Figure 5a were used to pump in the influent, pump out the effluent and for recirculation from the membrane to the sludge tank at a rate of 2000 $L.h^{-1}$.

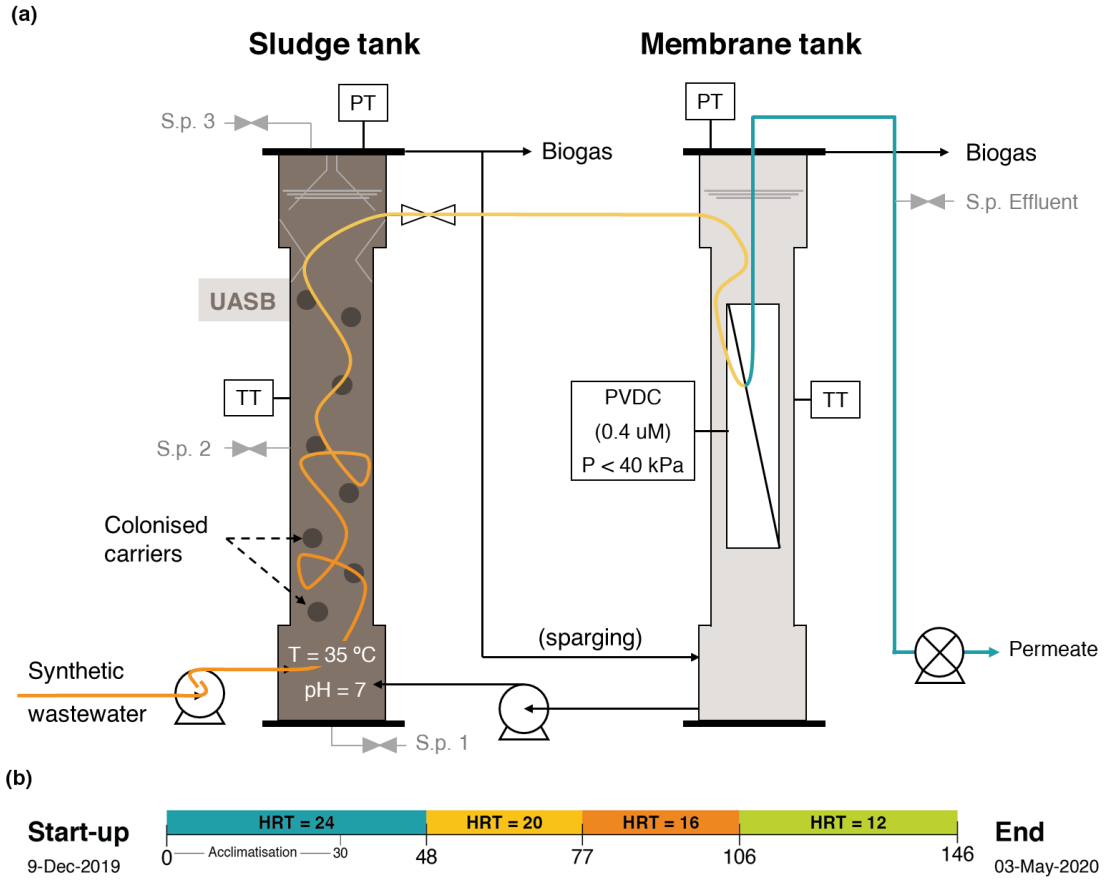

Figure 5. (a) AnMBR pilot reactor, and (b) the duration of its operation with the corresponding HRT changes. The pilot reactor is composed of a UASB sludge tank with spherical plastic carriers and of an external tank with an immersed membrane. The coloured line (orange to yellow to blue) simulates the liquid path inside the reactor with the gradient representing the treatment progress, PT and TT are the pressure and temperature transmits, respectively, and s.p., the sampling port.

The reactor has been operated for 146 days. The sludge tank was inoculated on December 9th 2019 (Day 0) with a mixed liquor suspended solids (MLSS) of 4.18 g.L$^{-1,}$ and it was allowed to acclimate over 30 days (Figure 5b). As displayed in Figure 5b, the HRT was set at 24 h for the first 48 days (phase 1), changed to 20 h in the following 29 days (phase 2), then to 16 h for additional 29 days (phase 3) and, at last, was altered to 12 h for the remaining 40 days (phase 4). The change of the HRT was determined based on the reactor's performance, meaning the stability of biogas production and COD removal, i.e. no further increment in biogas production and COD production for over 1-2 weeks. The solids retention time (SRT) was considered to be infinite as the sampled volume was small and the membrane retains the great majority of the solids.

The bioreactor was fed with synthetic wastewater, a mixture of organic and inorganic compounds as well as trace metals (Table A1) (Nopens et al., 2001). The organic loading rate (OLR) at which the influent was fed was of 1.19±0.05 gCOD.L^{-1}.d^{-1}, 1.49±0.07 gCOD.L^{-1}.d^{-1}, 2.00±0.06 gCOD.L^{-1}.d^{-1} and 2.58±0.04 gCOD.L^{-1}.d^{-1}, respectively for 24, 20, 16 and 12 hours. The organic matter content, measured as chemical oxygen demand (COD), was kept stable at an average of 1247±77 mgCOD.L^{-1}.

3.1.2. Performance monitoring

Sampling has been made for gaseous and liquid streams.

Biogas sampling was performed for the sludge tank biogas fraction and for the fraction coming out of the membrane tank. The gaseous samples were collected according to Table 4 from the sampling ports indicated in Figure 5.

Table 4. Summary of the biogas sampling characteristics (port location and frequency of sampling) and of the performed tests (volume and composition). The frequency for which the results have been analysed is displayed in Figure A1.

	Port	***Frequency***	***Volume***	***Composition***
Sludge tank	Biogas – sludge tank	Every day	✔	✔
Membrane tank	Biogas – membrane tank	Once a week *	✔	✔

* The reason being that the amount of biogas produced was reduced.

In order to be able to calculate the methane yield, the produced biogas volume was measured by a wet drum chamber gas meter (Ritter Apparatebau, Germany), and the qualitative gas composition analysed by gas chromatography on a thermal conductivity detector (TCD) (SRI 310C GC-TCD, SRI Instruments, USA). To calculate the methane yield ($CH_4\ yield$), the methane production had first to be estimated. For that, the average amount of methane ($\bar{x}_{CH_4}$) produced in both the biogas sludge and membrane tanks was obtained from Equation 3, considering the volume of biogas produced (V_{biogas}) and the average methane percentage ($\overline{\%CH_4}_{biogas}$), daily rationalized in Equation 4. This was added to the amount of dissolved methane in the effluent stream that was also obtained from Equation 3, however, in this case, the volume was taken as the volume of water treated per day ($V_{effluent\ dissolved\ per\ day}$) (quotient of the effective tank volume and the HRT time $\left(\frac{V_{eff}}{HRT}\right)$). Thus, the methane balance could be closed (Equation 4) and the methane production ($CH_{4_{production}}$) determined. It is relevant to note that the amount of dissolved methane ($x_{CH_{4_{effluent\ dissolved\ per\ day}}}$) was only calculated for some timepoints [1], but that the methane percentage ($\%CH_{4_{effluent\ dissolved}}$) accounted for very low values. In Table C1 those time points are presented associated with the corresponding $\%CH_{4_{effluent\ dissolved}}$ as well as, even if only for reference, the values for the percentage of methane inside the sludge ($\%CH_{4_{sludge\ tank\ dissolved}}$) and membrane ($\%CH_{4_{membrane\ tank\ dissolved}}$) tanks.

$$x_{CH_{4_i}}[L] = V_i\,[L] \times \%CH_{4_i}\,,$$
$$i = \{biogas\ sludge\ tank, biogas\ membrane\ tank, effluent\ dissolved\}$$

Equation 3

[1] COVID-19 lab restrictions

$$CH_{4_{production}}[L.d^{-1}] = \\ = \frac{\bar{x}_{CH_{4_{sludge\ tank}}}[L] + \bar{x}_{CH_{4_{membrane\ tank}}}[L]}{\Delta t\ [d]} + x_{CH_{4_{effluent\ dissolved}}}[L.d^{-1}] \quad \text{Equation 4}$$

Finally, the methane yield ($CH_4\ yield$) could be estimated (Equation 5) being the values for the COD feed to the reactor (COD_{feed}) directly measured. COD values are presented in Table 2.

$$CH_4\ yield\ \left[L.g\ COD_{feed}{}^{-1}\right] = \frac{CH_4\ production\ [L.d^{-1}]}{\frac{V_{eff}\ [L]}{HRT\ [d]} \times COD_{feed}\ [g.L^{-1}]} \quad \text{Equation 5}$$

As far as the efficiency in methane production is concerned, it is important to first take into account the value for the theoretical methane production ($Theoretical\ CH_4\ production$) for the consumed COD (Equation 6).

$$Theoretical\ CH_4\ production\ [L.d^{-1}] = \\ = \left(COD_{feed}\ [g.L^{-1}] - COD_{effluent}\ [g.L^{-1}]\right) \times \frac{V_{eff}\ [L]}{HRT\ [d]} \\ \times Y_{CH_4/COD}\ [L.g\ COD^{-1}] \quad \text{Equation 6}$$

Theoretically, 1 kg COD can be converted in 0.35 m^3 CH_4 ($Y_{CH_4/COD}$) (Lier et al., 2008). Therefore, the efficiency in methane production ($\%Efficiency\ CH_4\ production$) could be determined (Equation 7).

$$\%Efficiency\ CH_4\ production = \frac{CH_4\ production\ [L.d^{-1}]}{Theoretical\ \ CH_4\ production\ [L.d^{-1}]} \times 100\% \quad \text{Equation 7}$$

As far as the liquid samples are concerned, sampling was performed for the bulk of the sludge tank, for the effluent stream and for the biomass attached to carriers. The liquid samples were collected according to Table 5 from the sampling ports indicated in Figure 5.

Table 5. Summary of the liquid sampling characteristics (sampling port location, frequency of sampling and sampled volume) and of the performed tests (water quality for ammonia, phosphate, nitrite, nitrate and COD; cell quantification through flow cytometry (FCM)). The frequency for which the results have been analysed is displayed in Figure A1.

	Sampling port	***Frequency***	***V [mL]***	***Water quality***	***FCM***
Sludge tank bulk	1-3	Twice every week	100	✔	✔
Effluent	Effluent	Twice every week	50	✔	✔
Attached biomass	2**	Biweekly	30***	✗	✔

* Pumps were stopped and the sample collected through an aperture behind sampling port 2.

** Four carriers were removed, and 30 mL of PBS (1x) added.

In order to assess the efficiency of the bioreactor in the removal of organic matter and to monitor water quality, the concentration of water quality parameters (ammonia, phosphate, nitrate, nitrite and COD) had first to be determined. For that, sludge tank bulk and effluent stream samples were primarily digested via either one of the test kits presented in Table D1 in cuvette

test vials (Hach-Lange, Manchester, UK) and then, their concentrations were measured by spectrophotometry (HACH® DR2800 Spectrophotometer (Hach, Loveland, Colorado, USA).

The percentage of organic matter removal has been expressed in terms of COD removal efficiency ($\%COD\ removal\ efficiency$) and determined as follows:

$$\%COD\ removal\ efficiency = \frac{(COD_{feed}\ [g.L^{-1}] - COD_{effluent}\ [g.L^{-1}])}{COD_{feed}\ [g.L^{-1}]} \times 100\% \qquad \text{Equation 8}$$

As far as cell quantification is concerned, the samples present in Table 5 had first to be pre-processed. In particular, for the attached biomass samples there was a first extra pre-processing step for extraction of the biomass from the spherical plastic carriers. In order to achieve that, samples were vortexed for 1 min, then sonicated for 20 min at 25% frequency, pulsating at 2 s intervals using the QSonica® Q500 Sonicator (QSonica LLC, Newton, CT, USA), last vortexed one more time and, at last, the carriers removed. The remaining and general pre-processing steps intended to (i) sediment the sludge by centrifugating at 8000 g, for 10 min at room temperature, (ii) adequately dilute the supernatant with PBS (1X), and (iii) remove big solid particles (5 µm pore filter). The dilutions were of 10^3 times, for attached biomass samples, 10^2 times, for suspended ones, and 10^0 times, for the effluent ones.

Flow cytometry (FCM) analysis was performed in Accuri C6® (BD Bioscience, NJ, US), for monitoring purposes and BD FACSCanto™ II (BD Biosciences, San Jose, CA, USA), for cell quantification. The samples have been prepared for FCM analysis as shown in Figure 6.

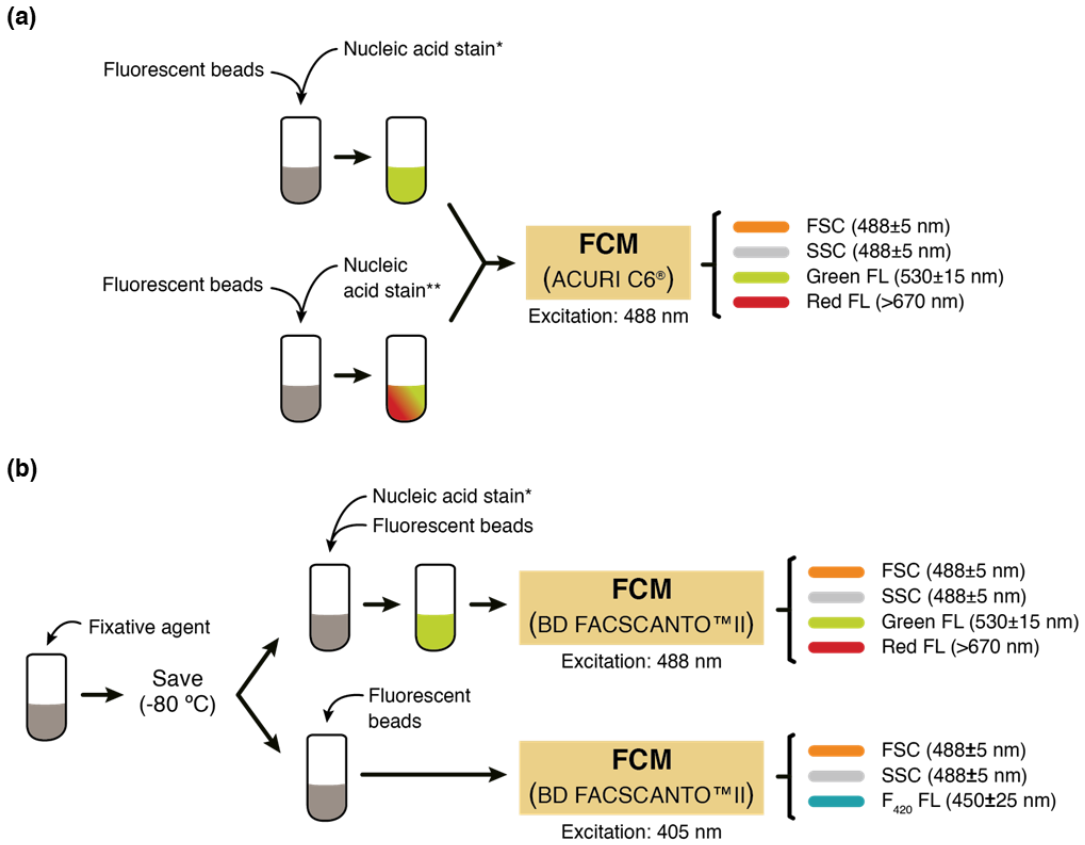

Figure 6. Sample preparation for flow cytometry and the characteristics of the analysis (excitation and optic filters used: forward and side scatter (FSC and SSC, respectively), and green, red and Cofactor F_{420} fluorescence (FL)), (a) for monitoring purposes of fresh samples with Accuri C6®, and (b) for cell quantification purposes with BD FACSCanto™ II. * SYBR Green I®; ** LIVE/DEAD BacLight®.

Samples for Accuri C6® were analysed fresh Figure 6a, and thus stained for a subsequent dilution to the one to be analysed. The staining was performed with SYBR Green I® (1:10000, Invitrogen Corp., Carlsbad, CA) and LIVE/DEAD BacLight® (1:1, Invitrogen Corp., Carlsbad, CA) stains, according to Gasol & Morán (2015). As samples for BD FACSCanto™ II could not be processed in the immediate time (i.e., between 1-2 h) and the staining of nucleic acids works better in aldehyde-fixed samples, these were firstly fixed (fixative agent composed of paraformaldehyde and glutaraldehyde) and only later, before running, divided in duplicates and either stained or not Figure 6b. One copy was then stained as mentioned in Gasol & Morán (2015) and the other not stained at all, so that a better cofactor F_{420} autofluorescence signal could be acquired.

FACSCanto™ II was equipped with a blue 488 nm Sapphire 488-20 (20 mW, Coherent) and a violet 405 nm iFLEX2000-P-1-405-0.65-30- NP (30 mW, Point Source). In the case of Accuri C6®, only a 488 nm solid-state blue laser (20 mW) was used. The 488 nm lasers were used for the analysis of forward scatter (FSC) (488/10), sidewards scatter (SSC) (trigger signal, 488/10), for SYBR Green I® fluorescence (530/30, FITC) and for red fluorescence (>670, PerCP-Cy™5.5). The 405 nm laser was used for the analysis of the fluorescence of the cofactor F_{420} in methanogenic archaea (450/50, Pacific Blue™);

Cell sample data was analysed using FlowJo® V10 (Flowjo, OH, USA).

In the software, to process stained samples' data, gates, i.e. delimited regions in the flow cytogram, were defined/drawn (Figure 7).

Firstly, with the help of a gate placed in a flow cytogram relating the side and forward scatters, events on the very edge have been removed as their sizes and morphological complexities were abnormal (Figure 7a).

As the green fluorescence denotes the presence of double stranded DNA, secondly, based on this fluorescence signal, the cell's population was selected (Figure 7b). The gate used was placed bellow the fluorescent bead's population in accordance with Gasol & Morán (2015). As far as effluent samples are concerned, the cell quantification was done only until this step, in terms of total cells (Figure B2).

For attached and suspended biomass, in this step (Figure 7b) it was already possible to discern some bimodal abundance of nucleic acid content, the high and low nucleic acid populations, HNA and LNA, respectively. However, for the attached and suspended biomass, by spreading the signal in the red fluorescence axis, as suggested by Gasol & Morán (2015), the borderline between these two populations becomes clearer. This borderline was demarked by a lower density of cells as shown in Figure 7c.

Additionally, subpopulations within the HNA and LNA domini have been selected to be traced as they exhibited some clustering properties and also that had potential to, later on, be more easily sorted (Figure 7d).

At last, unstained and stained samples would also had been quantified, according to Lambrecht et al. (2017) after removal of any outlier events as shown in Figure 7a. Nevertheless, both the stained and even the unstained samples had a clear lack of signal as shown in Figure B5, and thus, further quantification has not been carried on.

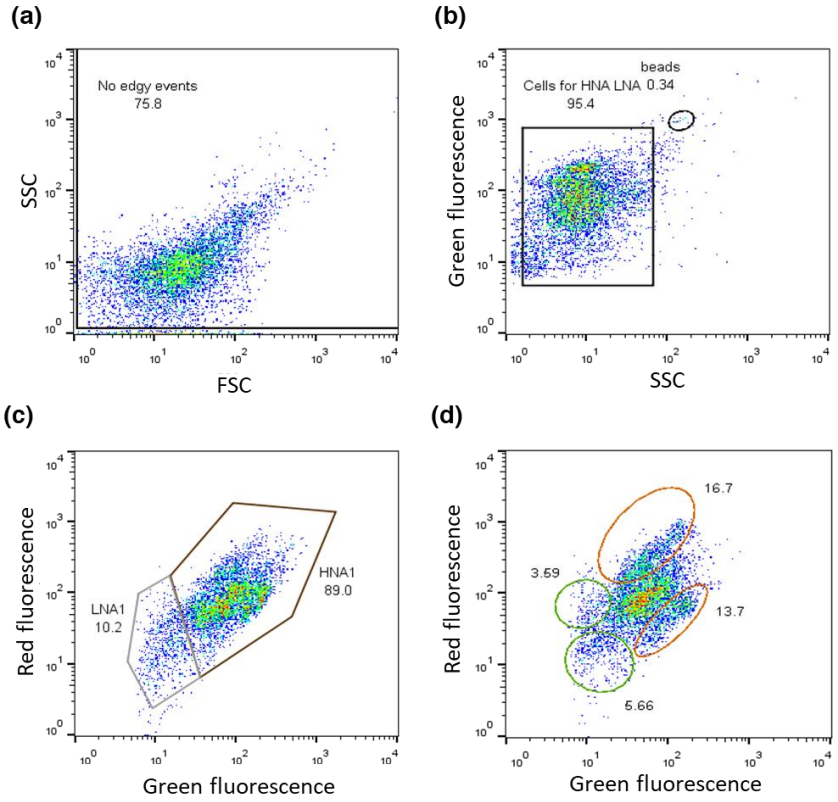

Figure 7. Gating strategy applied for quantification of cell events, (a) removal of all events on the edges in a forward and side scatters flow cytogram, FSC and SSC, respectively, (b) selection of the cell population based on the green fluorescence signal from nucleic acid stain, (c) quantification in HNA and LNA populations, respectively in the brown and grey polygonal gates, by spreading them in the red fluorescence axis, (d) traced subpopulations within the HNA and LNA populations, respectively in the orange and green elliptical gates.

The gating strategy applied enabled the determination of the number of events comprised in each gate ($no.\,gate\ events$). This value was converted to cells per mL by assuming each event as a single event, normalising by the volume of sample used by the FCM ($V_{sample\ analysed}$) and multiplying by the adequate dilution factors (DF) (Equation 9). The $V_{sample\ analysed}$ was calculated by the flow rate of the FCM and the time the device took to analyse it.

$$No.\,total\ cells\ per\ mL = \frac{no.\,gate\ events}{V_{sample\ analysed}\,[mL]} \times DF_{sample} \times DF_{fixing} \times DF_{staining+beads} \quad \text{Equation 9}$$

The aforementioned dilution factors have been estimated as in Equation 10 and Equation 11 taking into account the volume of the sample (V_{sample}), 0.4 mL, the volume of fixative agent (composed of paraformaldehyde (P) and glutaraldehyde (G); V_{P+G}) added, 0.18 mL, and the volume of stain ($V_{SYBR\ Green\ I}$) and beads (V_{beads}) added, 0.004 mL and 0.01 mL respectively. The dilution factor intrinsic to the sample preparation methodology (DF_{sample}) was 10^0 to the effluent, 10^2-10^3, to the suspended biomass, 10^3 to the attached biomass and 10^4 to the seed biomass.

$$DF_{fixing} = \frac{V_{sample}[mL] + V_{P+G}[mL]}{V_{sample}[mL]} \quad \text{Equation 10}$$

$$DF_{staining+beads} = \frac{V_{sample}[mL] + V_{SYBR\ Green\ I}[mL] + V_{beads}[mL]}{V_{sample}[mL]} \quad \text{Equation 11}$$

The median size of each gate was automatically determined by the analysis software. The given value was converted to cell diameter following the empirical calibration of Calvo-Díaz & Morán (2006) (Equation 12). This conversion uses the side scatter median value of the fluorescent beads of 1 µm diameter (added to all samples as an internal standard) to normalise the median size of the events from each gate.

$$Median\ cell\ size\ [\mu m] = 0.34 \times \log\left(\frac{median\ size\ of\ gated\ events}{median\ size\ of\ beads}\right) + 0.908 \quad \text{Equation 12}$$

As a final remark, samples have also been prepared for further assessment of volatile fatty acids (VFA), DNA and RNA. As mentioned before, one of the pre-processing steps was centrifugation and right after that step, part of the supernatant was used for cell quantification as described, the remaining, approximately 20 mL, were saved at -80 ºC for VFA analysis. As the volume collected was abundant the mentioned centrifugation step was performed into two falcon tubes. Hence, one of the pellets was saved at -80 ºC for future DNA extraction and analysis and to the other one added 3 mL of RNAlater® (Qiagen, Hilden, Germany) and saved first at 4 °C for 24 h and then at -80 °C for means of future RNA extraction and analysis.

3.2. Statistics

Statistical analysis has been employed to study the data collected from the pilot reactor operation and performance monitoring.

The significance was assessed either by a two-tailed t-test or one-way ANOVA, available in Microsoft® Excel® 2016 with a confidence interval of 95% assuming a normal distribution of the population. Thus, a probability (p) lower than 0.05 denotes samples heterogeneity while p values greater than 0.05, samples homogeneity. For the application of the correct t-test, the variance was firstly assessed by an f-test.

Matlab® (MathWorks) v. 9.8 was used to test the statistical significance of correlations in some of the dataset based on Pearson correlations. The confidence level was set at 95%. The results for the Pearson Correlation Coefficient, R, were only reported if $p<0.05$.

Chapter 4

Results and discussion

The following subsections are sorted in order to address the goals highlighted in the Project scope section. In the first subsection the operational performance of the reactor was characterised for all the different HRTs studied, finding the optimal one. In the second one the focus was on the study of the HNA and LNA clusters. As far as the third and last subsection of this chapter is concerned, the method was that of analysing the flow cytograms in the moment of the HRT change and when it stabilised. In addition, the period of reactor hibernation was also assessed as it could have impacted the microbial community.

As an introductory note for this chapter, and relevant for the analysis of its plots:

- Any sample taken directly from the sludge bulk is hereafter referred as "sludge". The analysed biomass from this type of sample corresponds to the suspended one;
- Samples derived from the extracted biomass attached to the carriers are hereafter designated as "biomass";
- Samples taken from the effluent stream, post-membrane treatment, hereafter named "effluent".

4.1. Operational performance

Throughout the 146 days of the experiment, multiple assays have been conducted to best characterise the reactor's performance and the microbiological community as described in the Methods' section.

In Figure 8, the operational performance parameters and information regarding gas composition have been plotted.

Overall, until day 30, the values of most of the parameters varied largely, with visible oscillations in the trends of the data (Figure 8, Figure 9 and Figure 10). The same type of behaviour was found until eight days after each HRT change except for the last HRT step (16h), in which that phase lasted for 24 days. Hence, only the stable domains of each HRT (except where noted) were considered for analysis and determination of the average values. Such domains, when relevant,

were highlighted in the figures with shaded rectangles that fit the Y-axis variation of the stable data points, disregarding the outliers.

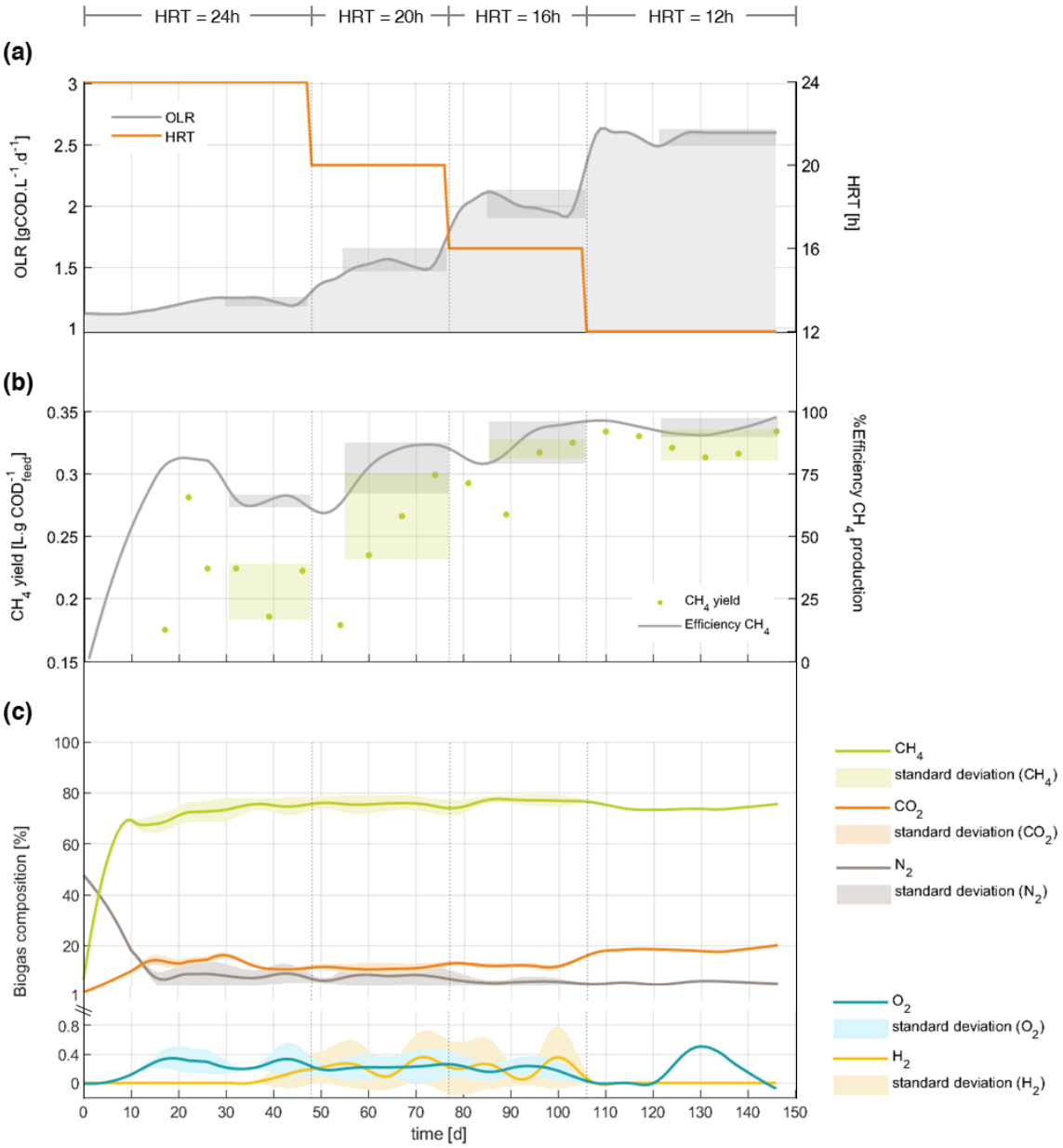

Figure 8. Operational performance of the pilot AnMBR for 146 days, (a) organic loading rate (OLR) and hydraulic retention time (HRT), (b) biogas yield and efficiency, the latter determined as a ratio between methane production and the expected stoichiometric methane production (considering the consumed organic matter; Methods' section), (c) biogas relative composition in terms of methane (CH_4), carbon dioxide (CO_2), nitrogen (N_2), oxygen (O_2) and hydrogen (H_2) (weekly average). The shaded rectangles represent the variation within the Y-axis on the considered stable domains.

An increase in OLR triggered a corresponding increase in methane production (Pearson R > 0.8, $p<0.05$; Figure 8a). Nevertheless, methane production did not stabilise for the first studied HRTs (24 and 20 hours; Figure 8b). Significant increase in methane production was only verified with the change of the HRT to 16 h (unpaired t-test, $p<0.05$; between 16-12 h HRTs, there were no significant changes).

The methane yield of the studied HRTs was of 0.20±0.02 $LCH_4.gCOD_{feed}^{-1}$, 0.29±0.02 $LCH_4.gCOD_{feed}^{-1}$, 0.325±0.008 $LCH_4.gCOD_{feed}^{-1}$ and 0.321±0.009 $LCH_4.gCOD_{feed}^{-1}$ for the experiments performed with HRT of 24, 20, 16 and 12 hours, respectively (Figure 8b). Any of these values was greater than the average of the reported ones for comparable AnMBRs (Table 1), 0.23±0.03 $LCH_4.gCOD_{feed}^{-1}$, except for the HRT of 24 h. For the 16 h and 12 h HRTs, methane yield was the most stable and the average methane production represented 94%±3% and 92±3%, respectively, of the maximum stoichiometrically-calculated value for the amount of organic matter consumed (Figure 8b). The reported values for this parameter are higher than the ones reported by Singh & Viraraghavan (2003) for municipal wastewater treatment with UASBs, 0.16-0.2 $LCH_4.gCOD_{removed}^{-1}$ [2]. This can be accounted for by differences in the operating temperatures. The temperatures of operation of that study (11-32 °C) were much lower than the ones used at KAUST (37 °C) and perhaps accounted for lower methanogenesis rate.

The decrease of the HRT to 12 h, and thus of the OLR, resulted in significant changes in the relative abundance of CO_2, N_2 and CH_4 in the biogas (one-way ANOVA, $p<0.05$; Figure 8c). The values for methane relative abundance in the biogas were of 75%±1% for the first two HRT tested (24 and 20 h) and of 77.0%±0.4% and 73.9%±0.9% for the last ones (16 and 12 hours; Figure 8c). These values, in particular the highest of 77.0%±0.4% for the 16 h HRT, were slightly below the range of the reported for methane produced under similar AnMBR operational conditions (80-90%; Chen et al., 2016). Nonetheless, these values are high above the ones reported for dedicated anaerobic digestion plants that treat municipal wastewater (60-65%; Korres et al., 2013). The values reported by the same author for other gaseous components (CO_2, 35-40%; N_2,<1-2%) also indicate that the production of N_2 by the reactor of this study is quite high, and the CO_2 (11.0%±0.3%-18.5%±0.9%) much lower than expected. Being N_2 a much more stable molecule in the atmosphere (practically inert), this balance is much more beneficial to the environment.

Another relevant factor of wastewater treatment reactors is their capacity to treat the influent streams. The efficiency of such treatment is well-characterized by the percentage of organic matter removed (%COD removal). In addition to that parameter, in this study, the levels of nitrite and nitrate are presented. Even though ammonia and phosphate were also monitored (Figure C1 for the effluent values and Table A2 for the influent ones), they are not so relevant for the AnMBR performance monitoring.

The decrease in HRT time leads to higher consumption of media. Thus, an increase in the nutrient levels and an adaptation of the microbial populations (cell number and/or enrichment or shift of subpopulations) are expected, particularly in the immediate time points after the HRT change. In Figure 9, the water quality parameters' performance is represented for both the sludge tank (concentration of the compound in bulk, partially treated, as used and perceived by the microorganisms) and the effluent stream (after full microbiological and membrane treatment). Therefore, it is implicit that if nutrients are consumed, the values of the compounds in the sludge bulk should always be greater than the ones in the effluent. The reverse trend can only be possible if such compounds are generated.

[2] Similar to $LCH_4.gCOD_{feed}^{-1}$ if the percentage of COD removed is high.

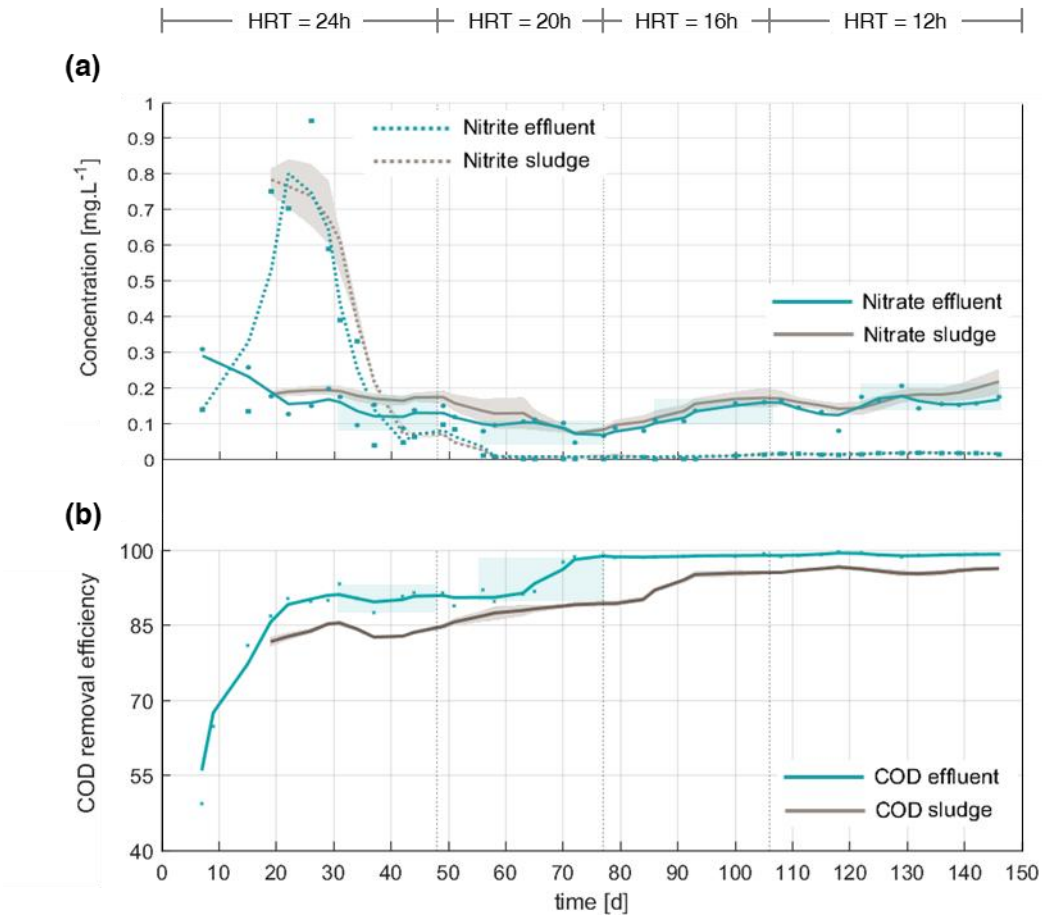

Figure 9. Water quality parameters throughout the 146 days of operation of the pilot AnMBR in the sludge tank bulk and effluent stream, (a) nitrite and nitrate levels, (b) removal efficiency of the chemically oxidisable organic matter measured as COD; values used to calculate this parameter can be consulted in Table C2. The trend lines are based on a moving average (n=3) filter applied to the results and the shaded irregular brown region demarks the standard deviation of the sludge measurements. The shaded rectangles represent the variation within the Y-axis on the considered stable domains of the effluent.

Nitrite is used for the anabolism of the denitrifying bacteria under anaerobic conditions, and thus, the residual fed amount (Table A2) was quickly depleted after the microbial community has adapted (probably after day 30) (Figure 9a). The total depletion of this compound is a positive outcome since it is one of the most toxic forms of nitrogen (Muhaidat et al., 2019).

The concentration of nitrate in the treated water have started to increase after the study of the 20 h HRT (one-way ANOVA, $p<0.05$; Figure 9a) which could be either due to a lack of metabolic activity or to a preference of the denitrifying bacteria for nitrite over nitrate, as both levels have risen with the HRT time reductions first to 16 h and then to 12 h.

The use of the carbon source became more efficient with the HRT time reduction being such efficiency measured as the percentage of COD removed (Figure 9b). The percentage of COD removed was of 91%±2% and 94%±4%, respectively, for the first two studied HRT times (24 and 20 hours) and of 98.8%±0.3% and 99.1%±0.2%, the highest, registered for the 16 and 12 hours HRTs, respectively. All the obtained values for this parameter are amongst all of the comparable AnMBR ones (Table 1) being the two highest ones even superior to the highest values reported for this parameter in the considered literature review, 96.6% (Cheng et al., 2019), and 97% (Ross et al., 1992).

While operating at 12h HRT, the reactor had to be put in hibernation mode for a few days [3]. Thus, the regime became anoxic during those days and less CH_4, but more CO_2 were produced (one-way ANOVA, $p<0.05$) (Figure 8c). As soon as the normal operation was resumed, there was a peak in the O_2 levels. It has been decided to keep the reactor operating for an extra amount of time in order to get the operational parameters more stable. Nevertheless, the given extra time was not enough as the values from the last timepoints of Figure 8 still oscillated. That was not the case for the levels of the water quality parameters (Figure 9) which, despite having oscillated with the change in the operating methodology, for those last timepoints, only nitrate levels have been significantly different when compared to other HRTs (one-way ANOVA, $p<0.05$).

All performance parameters considered, the best HRT was 16 h with an OLR of 2.00±0.07 g $COD.L^{-1}.d^{-1}$. With this HRT, very high levels of COD removal in the influent were attained (Figure 9b), and the methane yield was much more favourable than to any other time (Figure 8b). Additionally, it is important to note that the efficiency in methane production was at some points 97% (Figure 8b), which is a very satisfactory value for a pilot-scale AnMBR (Figure 1). Even though the 12 h HRT assessment failed, since some of the performance parameters' stability have been compromised, this HRT time had a small room for improvements after such surprising results from the 16 h HRT.

Steady-state performance in terms of methane yield and organic matter removal was observed at 12 and 16 hours HRTs. By considering that and that, even for the 20 h HRT, at least slow-growth microbial populations (e.g. methanogens) would have had already time to adapt, it was hypothesised that, for the quantified cells in the mentioned HRTS, the HNA to LNA ratio values would be more linear and constant during each correspondent HRT period. Contrarily, for the 24 h HRT, clearly non-steady operation, nothing could be hypothesised. In light of that, the values of the HNA:LNA ratios derived from flow cytometry could probably be used as a benchmark value to denote the optimal or steady-state operation of AnMBR.

4.2. Flow cytometry

The lower the HRT time, the higher the OLR and, consequently, the higher influx of nutrients provided to the system. If the microorganisms can bear the hydraulic stress induced by the changes, better conditions are met for their growth and replication. In Figure 10, several parameters of the cells that compose the system are depicted. Such information was extracted from flow cytometry data applying the gating strategy described in the Methods' section (Figure 7). In particular, in Figure 10d, the linear regression was applied only to the considered stable domains at each HRT. It was not possible to identify the stable domain for the HNA/LNA ratio for the 24 h HRT due to widespread of the data (very high value for the residual sum of squares (RSS), 35; the criteria to evaluate the fitting accuracy).

[3] The change to the 12 h HRT was followed by stringent restrictions at KAUST due to COVID-19 pandemic. The reactor had to be put in hibernation mode for few days as no one would be able to prepare the large daily volumes of media required (72 $L.d^{-1}$).

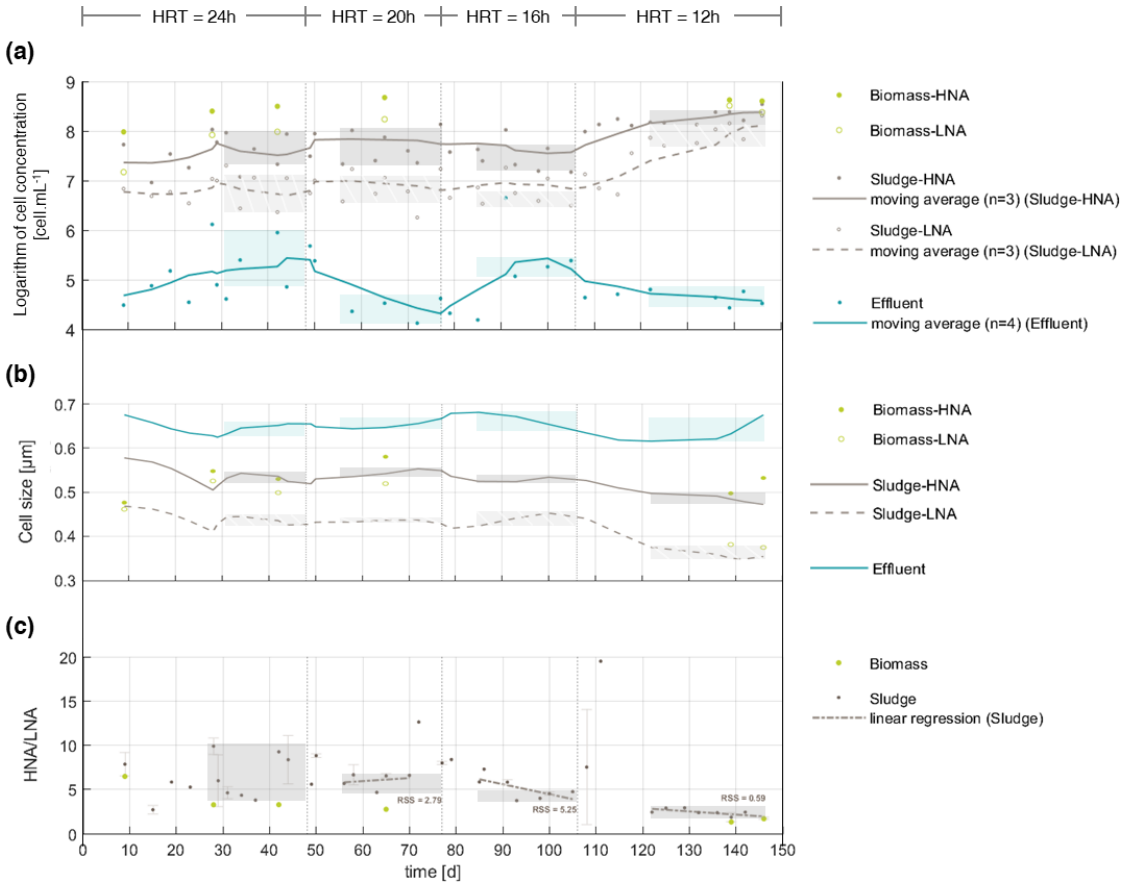

Figure 10. Microbial community behaviour during 146 days of operation of the pilot AnMBR, (a) logarithm of cell concentration, (b) median cell size, (c) relative content of HNA and LNA bacteria; linear regressions were applied only on the considered stable domains of each HRT using RSS to select the best fitting. The shaded rectangles represent the variation within the Y-axis on the considered stable domains.

Cell numbers and cell sizes (Figure 10a-b) in the sludge tank have remained relatively stable throughout all of the studied HRTs, the exception being the 12 h one in which significant changes have been observed (one-way ANOVA, $p<0.05$). There were no significant differences between the position inside the sludge tank (top, middle or bottom; one-way ANOVA, $p > 0.05$), but the cell numbers were the most coherent for the 24 h and 16 h HRTs (Figure C2).

It was possible to distinguish between LNA and HNA bacteria (Figure 10c) and to quantify those populations by using the gating strategy as explained in the Methods' section (Figure 7). In Figure 10c, it can be observed that not only did the HRT change provoke a large disequilibrium of the HNA and LNA relative populations (HNA:LNA ratio) in the sludge, but that it also led to a significant change of the HNA to LNA ratio value, the exception being the 24 h HRT (one-way ANOVA, $p<0.05$, only considering the last four time points from the 16 h HRT). For the 24 h HRT, the data was highly dispersed and no linear trend could be observed (high residual sum of squares (RSS) value, equal to 35), which was not the case for the remaining HRT. This can be possibly linked with the longer time of adaptation of the methanogens that may extend AnMBRs start-up times from 36 (Li et al., 2010) up to 100 days (Vincent et al., 2018). All the above considered, plus the results from the operational performance, it was confirmed that the HNA:LNA ratio could be used to assess the steady-state operation period of a reactor for the 12 and 16 hours HRTs. In the case of the 16 h HRT, by using this as a criterion, the steady-state operation could only be assumed for the last four timepoints which was also the period considered significant for the previously analysed HNA:LNA ratio's values and the period for which methane yield stabilised (Figure 8b).

The decrease of the sludge HNA to LNA ratio with the decrease of the HRT (Figure 10c) can be explained by either the HNA bacteria number having decreased at a faster pace than the LNA one, or the LNA bacteria having replicated much quicker than the HNA ones. The former seems to be the case for the 16 h HRT in which both average cell numbers decreased, the HNA at a faster rate and the latter is undoubtedly the case of the 12 h HRT. The flow cytograms (Figure 13) confirm that the HNA population has lost its relative importance with the change of the HRTs, increased OLR, and that in the 16 h HRT the suspended biomass got its LNA population enriched. The initial (seed sludge) and ending timepoints are displayed in Figure B3 and Figure B4, respectively.

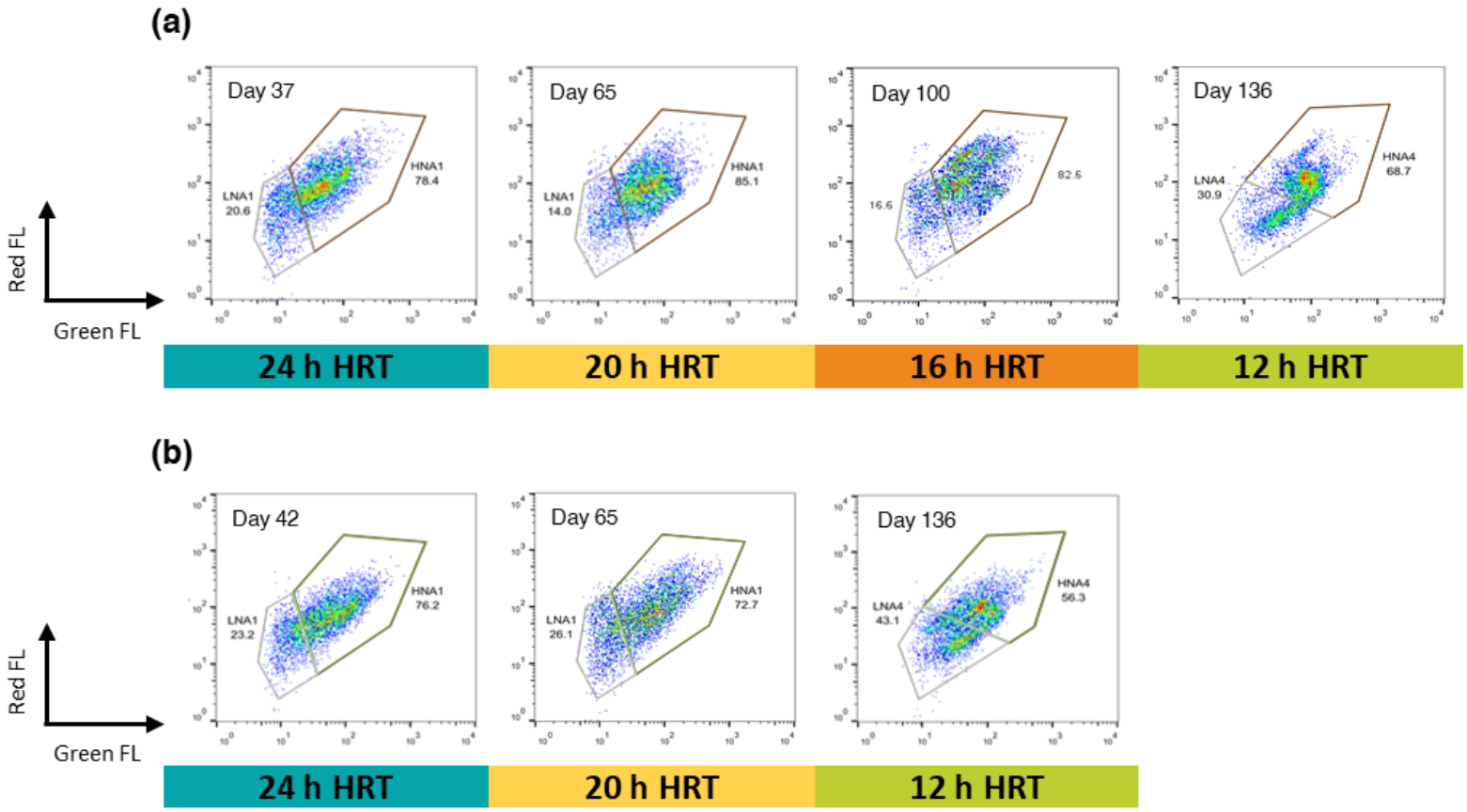

Figure 11. Flow cytograms from sludge tank samples representative of each HRT, (a) suspended biomass, (b) attached biomass. The Y-axis and X-axis represent the intensity of red and green fluorescence detected, respectively. The values near the polygonal gates represent the relative abundance of the events inside the gate from the total number of events. The sampling of attached biomass for the 16 h HRT has not been performed (Figure A1).

The attached biomass always had a larger number of cells than the suspended one ("sludge") (Figure 10a). In particular, its LNA population had much higher cell numbers and cell sizes (Figure 10b) in comparison to sludge LNA population. The enrichment in cell numbers indicates that LNA population (i) grows better if attached to a surface, or (ii) needs to be protected from the hydraulic stresses, or even (iii) that it needs to be interacting with other cell metabolites in a more convenient spatial arrangement. The cell size enrichment can either indicate that the cells could simply increase their cell size more or that different subpopulations exist within the LNA population. By the analysis of Figure 11, it is possible to see that the attached biomass had a slightly more enriched portion in the upper and right zones of the LNA gate rather than the suspended biomass. The lack of biomass samples does not allow to be confident about the mentioned slight enrichment, and only sorting and sequencing such populations could, in a definite way, validate the referred suppositions. In Figure 11b it is also possible to verify that the attached biomass did not lose any core subpopulations substantially throughout the various HRTs tested, the exception being the 12 h HRT due to the harsher conditions the reactor met. During this last HRT, the suspended biomass (Figure 11a) had, in comparison to the attached, a more substantial presence of a subpopulation that is between the LNA and HNA gating.

4.3. Microbial dynamics

4.3.1. Main microbial subpopulations at different HRTs

The decrease of the HRT time increased the OLR and the rate at which the nutrients were fed to the reactor. Consequently, better conditions were provided to the cells if they could bear the hydraulic stress also induced.

During operation at 16 h HRT, the relative methane abundance increased (Figure 8c). This increase was significant for the methane yield (unpaired t-test, $p<0.05$) (Figure 8b) which might be linked with a better performance of the methanogenic archaea. As shown in Figure C1, during the 16 h HRT, the effluent has also augmented its ammonia levels noticeably, increasing the gap with the sludge values, and thus, the cause cannot be merely attributed to the OLR increase; ammonia has been generated by the cells. Such behaviour indicates a preference for the 'protein pathway' (Figure 1) and denotes the existence of a more active fermentative bacterial population. As fermentative bacteria are fast growing microorganisms (Lier et al., 2008) and denote, in general, an increasing nucleic acid content (Table 2), they are expected to belong to the HNA population.

In Figure 12, several flow cytograms display how some of the microbial subpopulations of the HNA (highlighted in orange) and LNA populations (highlighted in green) shifted throughout the different studied HRTs (12 h HRT was not shown due to the peculiar problems this HRT had). Two main subpopulations of each of the HNA and LNA groups have been highlighted: one with a stronger emission of red fluorescence (higher PerCp value associated), and the another with weaker fluorescence, both with relatively the same green fluorescence signal (FITC). These tracked subpopulations have been chosen since they are more easily identifiable and sensitive to changes in the flow cytogram. In addition, their location favours the possible future sorting.

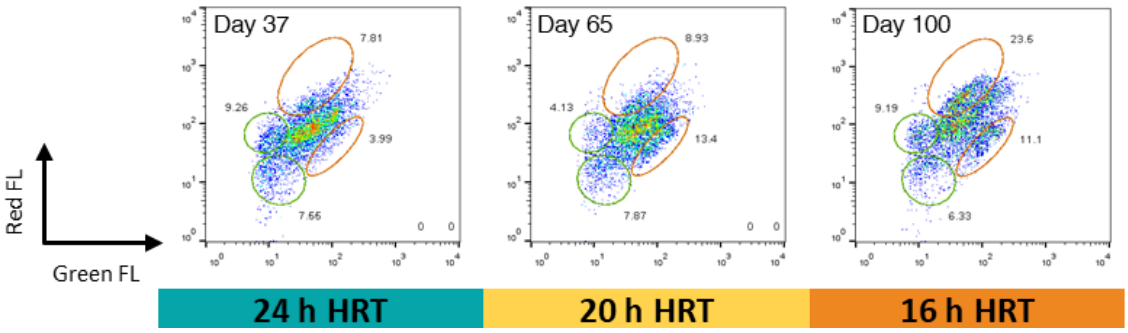

Figure 12. Microbial subpopulations inside the HNA and LNA populations (orange and green ellipses, respectively) from the sludge tank bulk across different HRTs (24 h, 20 h and 16 h). The values near the elliptical gates represent the relative abundance of the events inside the gate from the total number of events.

In Figure 12, it is possible to observe a noticeable decrease of the strongly red fluorescent LNA subpopulation from the 24 to 20 hours HRTs and an increase from the 20 to 16 hours HRTs (highlighted with green ellipses). The dimmest red fluorescent LNA subpopulation has slightly decreased from the 24 and 20 h HRTs to the 16 h one. The reduction of the dimmest red fluorescent LNA subpopulation was probably due to the denitrifying bacteria adaptation during this period as nitrate levels have also risen with the decrease of the HRT time (Figure 9a). As far as the HNA is concerned, the strongly red fluorescent subpopulation has substantially increased from the 20 and 24 hours HRTs to the 16 h one.

For the 16 h HRT, the increase of the above referred strongly red fluorescent HNA and LNA subpopulations might be linked with both the fermentative bacteria and methane-producing archaea. Identifying the bacteria which belong to each subpopulation is only possible through sorting and sequencing of both subpopulations. Nevertheless, the former could be due to fermentative bacteria by the aforementioned fact that these bacteria seem metabolically more active and also because ammonia levels have risen inside the reactor (Figure C1,effluent values), denoting a preference for the protein pathway. The increasing LNA subpopulation could be associated with methanogens as the methane yield has increased during this period (Figure 8) and archaea have the lowest nucleic acid content among all the microbial community (Table 2).

The number of cells present in the effluent stream has oscillated throughout the different HRTs. Such oscillation was particularly significant on the HRT change from 20 h to 16 h (unpaired t-test, $p<0.05$) (Figure 10a). Even though effluent cell sizes had no significant variation (one-way ANOVA, $p > 0.05$), the composition of the effluent has changed, as shown in Figure 13.

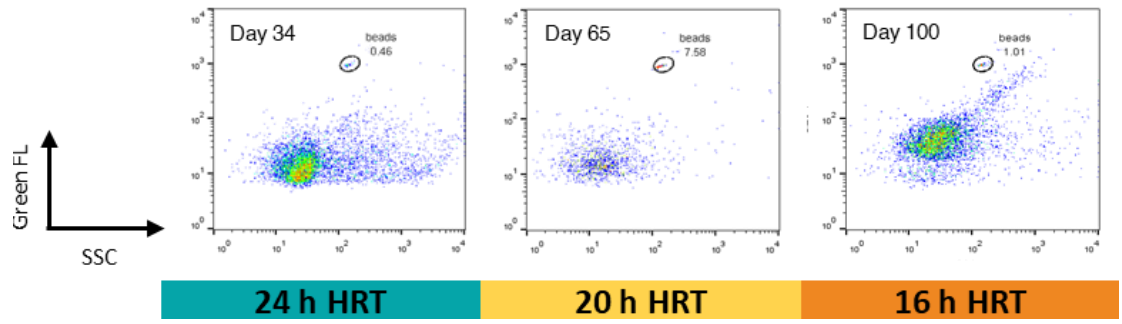

Figure 13. Flow cytograms from the effluent stream representative of each HRT. The Y-axis and X-axis represent the intensity of the green fluorescence detected, and the sidewards scatter (SSC), respectively. The values near the elliptical gates represent the relative abundance of the events inside the gate from the total number of events.

The noticeable changes in the effluent composition (Figure 13) led to the establishment of a gate positioned around the most relevant effluent population which is in the same placement as for the HNA and LNA gating strategy (Methods' section). Doing so enabled the further implementation of an HNA:LNA gating strategy (Figure 14).

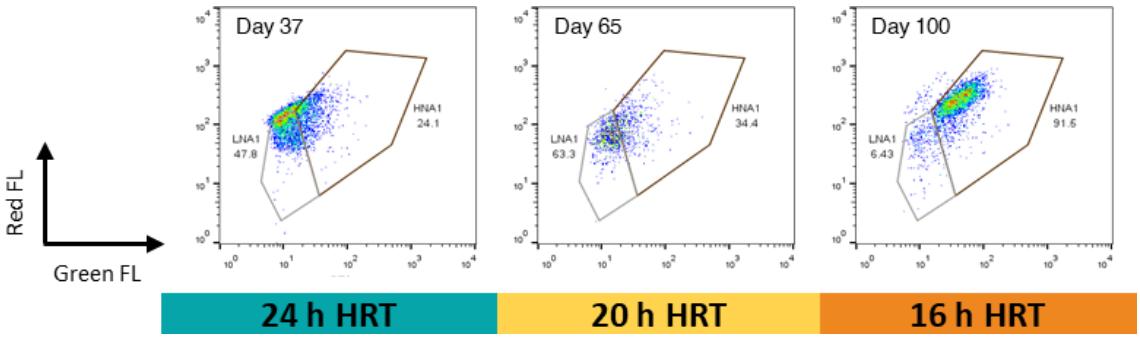

Figure 14. Flow cytograms from the effluent stream representative of each HRT, quantified in terms of HNA and LNA. The Y-axis and X-axis represent the intensity of the red and green fluorescence detected, respectively. The values near the polygonal gates represent the relative abundance of the events inside the gate from the total number of events.

Nevertheless, the results were not conclusive. Despite the correlation of the HNA enrichment in the effluent at the 16 h HRT (Figure 14) with the previously mentioned increase of strongly red fluorescent subpopulation (Figure 12), any other change (whether microbial or operational) might explain any effluent-driven microbiological behaviour.

4.3.2. Microbial community shift upon changes in HRT

Upon a change in HRT, there was a sudden enrichment of the HNA and LNA populations (Figure 10a), suggesting that both have reacted to the hydraulic stress. In addition, the HNA population momentarily experienced a decrease in its cell size (Figure 10b). Cell numbers-wise, the LNA population throughout the 24 h, 20 h and 16 h HRTs did not react to the HRT changes (one-way ANOVA, $p > 0.05$) only, in the last HRT (12 h), having decreased (Figure 10a) (probably due to the hibernation of the reactor and consequently anoxic regime). Immediately after the change of any HRT, except the 12 h one, the methane yield and N_2 levels decreased (Figure 8b-c).

In Figure 15, it is possible to track the evolution of the highlighted subpopulations in the HNA and LNA domains (orange and green ellipses, respectively, the same as in the previous subsection).

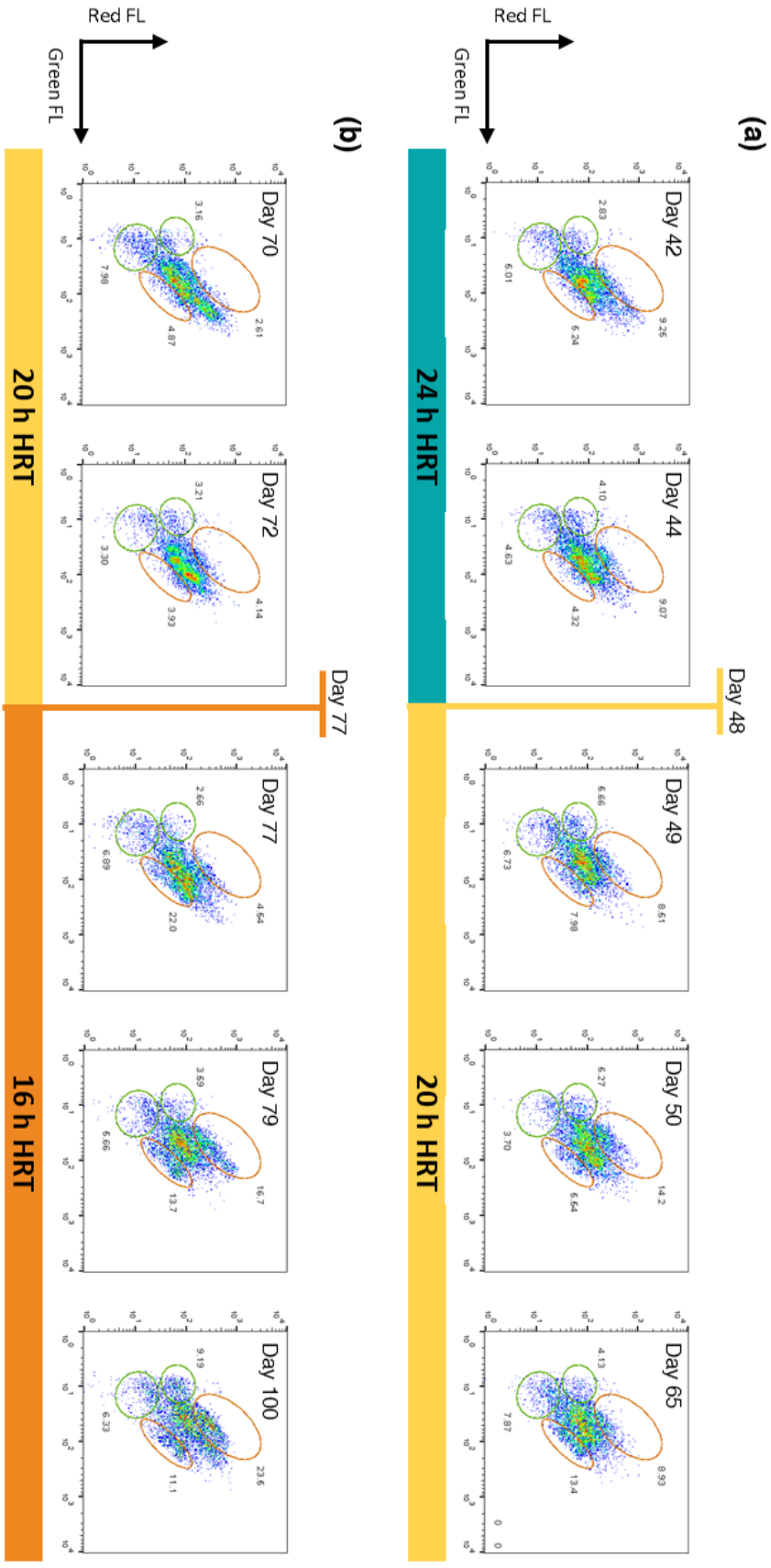

Figure 15. Microbial subpopulations inside the HNA and LNA populations (orange and green ellipses, respectively) from the sludge tank bulk, immediately before and after an HRT change from, (a) 24 h to 20 h, (b) 20 h to 16 h. The values near the elliptical gates represent the relative abundance of the events inside the gate from the total number of events.

In Figure 15, the enrichment of the dimmest red fluorescent HNA subpopulation is denoted for both HRT changes. By lack of more information from performance parameters that might as well have increased, it is not possible to do any suppositions regarding the nature of this subpopulation. Sorting and sequencing it would thus be a relevant alternative. The only additional information regarding such subpopulation is that it has a lower cell size, as the median size decreased (Figure 10b). As for the LNA subpopulations, there were only changes (increases) in the strongly red fluorescent subpopulation with the change of the HRT from 24 to 20 hours (Figure 15a).

As both N_2 and methane yield decreased right after HRT changes from 24 to 16 hours (Figure 8b-c), denitrifying and methanogenic subpopulations could have had reduced its numbers. However, in both HNA and LNA groups, there were no subpopulations that had that type of behaviour. Perhaps the increase of replication rate from the HNA population (Figure 10c) might have shortly mitigated N_2 and methane production (plus methane yield, consequently).

The effluent stream had no clear cell patterns in terms of size and number (Figure 10b-c). As differences in cell size were not expected to be relevant, the flow cytograms for this parameter (Figure 16) are a result of the direct application of the same HNA and LNA gating strategy as in the previous subsection (Figure 14).

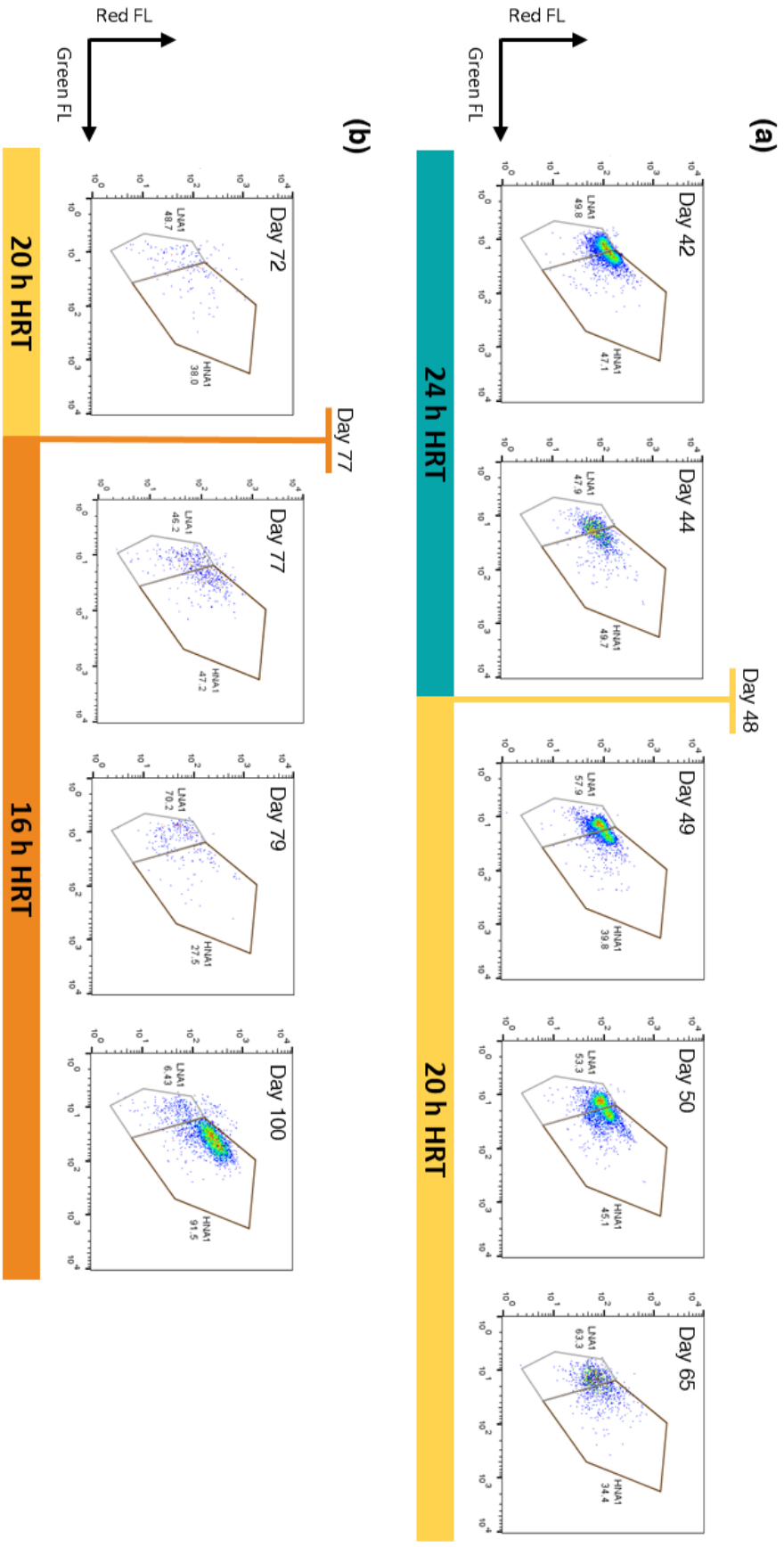

Figure 16. Flow cytograms from the effluent stream immediately before and after an HRT change and quantified using the HNA and LNA gating strategy. (a) HRT change from 24 h to 20 h, (b) HRT change from 20 h to 16 h. The Y-axis and X-axis represent the intensity of the red and green fluorescence detected, respectively. The values near the polygonal gates represent the relative abundance of the events inside the gate from the total number of events.

From the plots of Figure 16, it was not possible to gather any new insights in the system, and thus the application of flow cytometry with the purpose of distinguishing any specific subpopulations in the effluent was not fulfilled. Nevertheless, for the HRT change from 24 to 20 hours, it was possible to notice the aforementioned enrichment of the LNA population (Figure 16a).

4.3.3. Reactor hibernation

The aforementioned anoxic regime in the 12 h HRT induced a disequilibrium between the HNA and LNA populations in sludge samples: the HNA bacterial population increased its numbers at a disproportionate pace over the LNA population, whose numbers decreased (Figure 10c). Even though the HNA and LNA subpopulations analysis shown here does not yield definitive conclusions, it can be postulated that the HNA population has more quickly reacted to this change. Taking into consideration that HNA bacteria, are a more metabolically active group (Belzile et al., 2008) and that, according to Win et al. (2016), homoacetogenic bacteria tend to rapidly adapt to the shocks induced in the system competing with methanogens under shock period, homoacetogenic bacteria may be part of the HNA population.

As proteins are complex molecules, it is a greater metabolic effort to break them down rather than carbohydrates. Under substrate limitations, according to (Gallert & Winter, 2005), acetogenic bacteria will be more active than acidogenic ones, thus diverting the pathway to produce acetate, H_2 and CO_2 instead of volatile acids. By assuming this, more CO_2 would be produced, as confirmed in Figure 8c for this HRT (12 h), and less ammonia would be produced, which was the case with the effluent values becoming closer to sludge's ones at this stage (Figure C1).

Throughout this hibernation phase, denitrifying bacteria were also ultimately obliged to rely on the nitrate respiration (Lier et al., 2008), which may explain the greater consumption of this nutrient (Figure 9a).

To follow the evolution of subpopulations in the HNA and LNA populations, in Figure 17, some were highlighted (orange and green ellipses, respectively, the same as in the previous subsection).

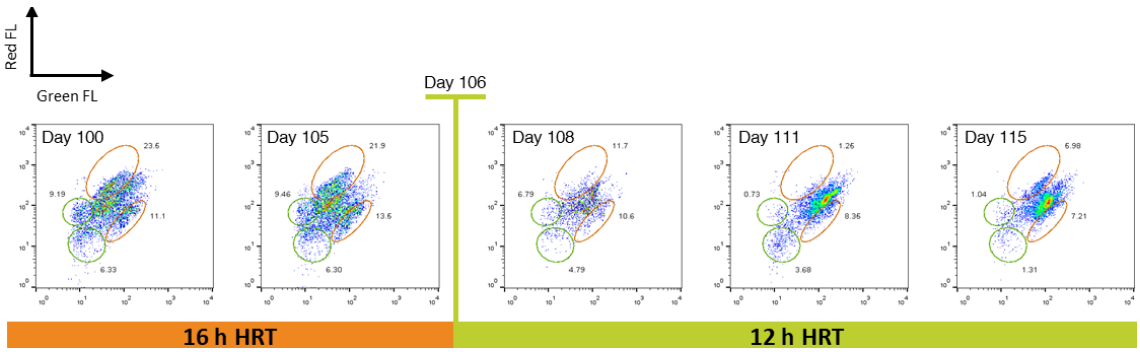

Figure 17. Microbial subpopulations inside the HNA and LNA populations (orange and green ellipses, respectively) from the sludge tank bulk, immediately before and after the HRT change from 16 h to 12 h. The values near the elliptical gates represent the relative abundance of the events inside the gate from the total number of events.

From the analysis of Figure 17, it is possible to conclude that the anoxic regime and/or hydraulic stress profoundly affected the microbial community. There was a progressive enrichment of the highlighted dimmest red fluorescent HNA population and a gradual decrease of both the other highlighted HNA subpopulation (with stronger red fluorescence emission) and of the whole LNA population. These shifts may be key to understand the composition of these two big groups, the HNA and the LNA ones.

As mentioned before, denitrifying microorganisms struggled throughout this anoxic phase, while acidogenic bacteria thrived. Indeed, denitrifying bacteria are known for their slow metabolic activity while acidogenic are more metabolically active (Lier et al., 2008). Therefore, there is likely a link which can be established between the former and the LNA population. A similar link between acidogenic bacteria and the subpopulation highlighted with weaker red fluorescence may be established. Sorting and sequencing of the most affected populations at this stage would be beneficial to understand better how microbial community has adapted to the change and validate this supposition.

As a final remark, unstained and stained samples have also been studied to assess the natural fluorescence from cofactor F_{420} from archaeal methanogens (Figure B5). Nevertheless, no substantial fluorescence signal was obtained by cofactor F_{420} despite it being known that methanogenic archaea were present in the system (high methane production denoted in Figure 8b). This lack of F_{420} signal might be due to either a FCM-related problem, or due to the low relative abundance of these methanogens in the anaerobic membrane bioreactor (Cheng et al., 2019), thus being obscured in the gated regions of flow cytogram. Additionally, some distinctive HNA and LNA subpopulations have been found and highlighted in Figure B6. By sorting and sequencing such subpopulations, better insight on the microbial community of the reactor would be possible as well as to start building a microbial fingerprinting profile.

Chapter 5

Conclusions

5.1. Contributions of this study

The AnMBR process, as a biological treatment, has its treatment performance determined by the microbial community that thrives in the bioreactor. Process optimisation, i.e. improvement of process control and stability, therefore requires a more in-depth knowledge of microbial dynamics so that operators are be able to make more rational decisions throughout the operation. The most well-established methods to assess microbial profile and changes are laborious, expensive and slow. In light of these limitations, flow cytometry emerges as a much faster and convenient alternative. By clustering the bacteria in two groups, the high and low nucleic acid bacteria, HNA and LNA respectively, the analysis of the system is further simplified, thus allowing for a more practical decision-driven methodology for AnMBRs operators.

With this work, we proved that flow cytometry, as a quick analytic tool by its own nature, can provide relevant information about the microbial community in a timely manner, making it ideal for applications in AnMBRs.

Prior to any FCM analysis, bioreactor operation was validated, from which additional insight was gained. It was observed that the bioreactor operation was successful with a high continuous production of biogas and COD removal percentage for all the studied HRTs (24, 20, 16 and 12 hours. Within the mentioned HRTs, only at the 12 and 16 hours ones there was a, even though short-lived, steady-state operation denoted by a stable methane yield. As during the 12 h HRT the reactor has undergone an hibernation period, the 16 h HRT was selected as the optimal time due to the high methane yield and the highest COD removal percentage, 0.325 ± 0.008 $L.gCOD_{feed}^{-1}$ (corresponding to the most efficient methane production from the fed organic matter, 82%) and 98.8%±0.3%, respectively, greater values than to any comparable AnMBRs from bench to full-scale.

For suspended and attached biomass, quantification of the HNA and LNA bacteria was possible. The use of the HNA to LNA ratio as a measure of the steady-state performance of the bioreactor is a promising approach. A linear correlation with time was observed for three of the

latest studied HRTs, 20, 16 and 12 hours, and steady-state in other operational parameters was observed for the 16 and 12 hours HRTs.

Inside the HNA and LNA clusters, other subpopulations have been traced. The changes on these subpopulations have been correlated with operational parameters, including the change of HRT.

The fluorescence of the cofactor F_{420} from archaeal methanogens could not be assessed in the flow cytograms which may either denote the low abundance of this population in the AnMBR, or an FCM-related problem.

Globally, this work has demonstrated that FCM and HNA/LNA assessment have great potential as simpler and quicker methods for analysing microbial changes in AnMBRs. In particular, the HNA to LNA ratio could denote some steady-state operation which could be used for process control. By identifying (sequencing) the microorganisms from relevant (sub)populations, more insight would be obtained for the use of this tool (FCM) in denoting the dynamics of these cells and validating the influence of any correlated operational parameters.

Nevertheless, the problem studied is very complex and it is necessary to take into account the limitations and simplifications involved such as the success of gating workflow that is heavily reliant on the researcher expertise, frequently to a problematic degree, as it is a manual step.

5.2. Future work

For future work, it would be of paramount importance the sorting and sequencing of all the interesting subpopulations. Sequencing also what was gated out could be additionally insightful.

It is also important to verify the correlation of the HNA to LNA ratio with the steady state performance of the bioreactor. For this, in the future, smaller scale experiments could be done and designed for longer periods of time to guarantee the stabilisation of the operational parameters. The FCM sample preparation methodology also needs to be re-evaluated and scrupulously well-done so that the patterns in the flow cytograms are uniform.

It would be necessary to investigate the problems that might have impacted cofactor F_{420} fluorescence assessment by reconfiguring the optics system of the FCM or changing equipment and running the samples once more.

Performing a volatile fatty acids' analysis may help validate the established correlations between operational parameters and microbiological (sub)populations and evaluating total solids, would help in better characterising treatment efficiency

At last, it would be interesting to re-evaluate the 12 h HRT, despite the exciting results obtained with the 16 h one. The reactor must be able to adapt to the needs of municipal wastewaters, which vary a lot. By choosing one HRT as the standard for operation, it is still valuable to know that, if needed, with a lower HRT, effluent treatment quality and gas production would not be undermined.

References

Akunna, J. C., Bizeau, C., & Moletta, R. (**1992**). Denitrification in anaerobic digesters: Possibilities and influence of wastewater COD/N-NOX ratio. *Environmental Technology (United Kingdom)*, *13*(9), 825–836.

Ali Shah, F., Mahmood, Q., Maroof Shah, M., Pervez, A., & Ahmad Asad, S. (**2014**). Microbial Ecology of Anaerobic Digesters: The Key Players of Anaerobiosis. *The Scientific World Journal*, *2014*, 1–21.

Bashiri, G., Antoney, J., Jirgis, E., Shah, M., Ney, B., Copp, J., Stutely, S., Sreebhavan, S., Palmer, B., Middleditch, M., Tokuriki, N., Greening, C., Baker, E., Scott, C., & Jackson, C. (**2018**). A revised biosynthetic pathway for the cofactor F 420 in bacteria. *BioRxiv*, 1–41.

Belzile, C., Brugel, S., Nozais, C., Gratton, Y., & Demers, S. (**2008**). Variations of the abundance and nucleic acid content of heterotrophic bacteria in Beaufort Shelf waters during winter and spring. *Journal of Marine Systems*, *74*(3–4), 946–956.

Berkessa, Y. W., Yan, B., Li, T., Tan, M., She, Z., Jegatheesan, V., Jiang, H., & Zhang, Y. (**2018**). Novel anaerobic membrane bioreactor (AnMBR) design for wastewater treatment at long HRT and high solid concentration. *Bioresource Technology*, *250*(September 2017), 281–289.

Bohdziewicz, J., Neczaj, E., & Kwarciak, A. (**2008**). Landfill leachate treatment by means of anaerobic membrane bioreactor. *Desalination*, *221*(1–3), 559–565.

Boster Biological Technology. (n.d.). *Flow cytometry fundamental principle*. Retrieved September 22, 2020, from https://www.bosterbio.com/protocol-and-troubleshooting/flow-cytometry-principle

Bouvier, T., Del Giorgio, P. A., & Gasol, J. M. (**2007**). A comparative study of the cytometric characteristics of high and low nucleic-acid bacterioplankton cells from different aquatic ecosystems. *Environmental Microbiology*, *9*(8), 2050–2066.

Calvo-Díaz, A., & Morán, X. A. G. (**2006**). Seasonal dynamics of picoplankton in shelf waters of the southern Bay of Biscay. *Aquatic Microbial Ecology*, *42*(2), 159–174.

Chan, Y., Chong, M., Law, C., & Hassell, D. G. (**2009**). A Review on Anaerobic–Aerobic Treatment of Industrial and Municipal Wastewater. *Chemical Engineering Journal*, *155*, 1–18.

Chen, C., Guo, W., Ngo, H. H., Lee, D. J., Tung, K. L., Jin, P., Wang, J., & Wu, Y. (**2016**). Challenges in biogas production from anaerobic membrane bioreactors. *Renewable Energy*, *98*, 120–134.

Cheng, H., Cheng, D., Mao, J., Lu, T., & Hong, P. Y. (**2019**). Identification and characterization of core sludge and biofilm microbiota in anaerobic membrane bioreactors. *Environment International*, *133*.

Cheng, H., & Hong, P.-Y. (**2017**). Removal of Antibiotic-Resistant Bacteria and Antibiotic Resistance Genes Affected by Varying Degrees of Fouling on Anaerobic Microfiltration Membranes. *Environmental Science & Technology*, *51*(21), 12200–12209.

Cossarizza, A., Chang, H.-D., Radbruch, A., Acs, A., Adam, D., Adam-Klages, S., Agace, W., Aghaeepour, N., Akdis, M., Allez, M., Almeida, L., Alvisi, G., Anderson, G., Andrä, I., Annunziato, F., Anselmo, A., Bacher, P., Baldari, C., Bari, S., & Richter née Gruber, L. (**2019**). Guidelines for the use of flow cytometry and cell sorting in immunological studies. *European Journal of Immunology*, *49*, 1457–1973.

Dvořák, L., Gómez, M., Dolina, J., & Černín, A. (**2016**). Anaerobic membrane bioreactors—a mini review with emphasis on industrial wastewater treatment: applications, limitations and perspectives. *Desalination and Water Treatment*, *57*(41), 19062–19076.

Faisal I. Hai, Kazuo Yamamoto, C.-H. L. (**2013**). *Membrane Biological Reactors*. IWA publishing.

Gallert, C., & Winter, J. (**2005**). Bacterial Metabolism in Wastewater Treatment Systems. In *Environmental Biotechnology* (pp. 1–48). John Wiley & Sons, Ltd.

Gao, W. J., Leung, K. T., Qin, W. S., & Liao, B. Q. (**2011**). Effects of temperature and temperature shock on the performance and microbial community structure of a submerged anaerobic membrane bioreactor. *Bioresource Technology*, *102*(19), 8733–8740.

Gasol, J. M., & Morán, X. A. G. (**2015**). Flow Cytometric Determination of Microbial Abundances and Its Use to Obtain Indices of Community Structure and Relative Activity. *T.J. McGenity et Al. (Eds.), Hydrocarbon and Lipid Microbiology Protocols, Springer Protocols Handbooks*, *2016*, 159–187.

Givan, A. L. (**2001**). Principles of flow cytometry: An overview. *Methods in Cell Biology*, *63*(63), 19–50.

Gouveia, J., Plaza, F., Garralon, G., Fdz-Polanco, F., & Peña, M. (**2015**). Long-term operation of a pilot scale anaerobic membrane bioreactor (AnMBR) for the treatment of municipal wastewater under psychrophilic conditions. *Bioresource Technology*, *185*, 225–233.

Greening, C., Ahmed, F. H., Mohamed, A. E., Lee, B. M., Pandey, G., Warden, A. C., Scott, C., Oakeshott, J. G., Taylor, M. C., & Jackson, C. J. (**2016**). *Physiology, Biochemistry, and Applications of F 420-and F o-Dependent Redox Reactions*. *80*(2), 451–493.

Hammes, F., & Egli, T. (**2010**). Cytometric methods for measuring bacteria in water: advantages, pitfalls and applications. *Analytical and Bioanalytical Chemistry*, *397*(3), 1083–1095.

Harb, M., & Hong, P. Y. (**2017**). Anaerobic Membrane Bioreactor Effluent Reuse: A Review of Microbial Safety Concerns. *Fermentation*, *3*(3), 39.

Harb, M., Xiong, Y., Guest, J., Amy, G., & Hong, P.-Y. (**2015**). Differences in microbial communities and performance between suspended and attached growth anaerobic membrane bioreactors treating synthetic municipal wastewater. *Environ. Sci.: Water Res. Technol.*, *1*(6), 800–813.

Hawley, T. S., & Hawley, R. G. (**2011**). *Flow Cytometry Protocols* (3rd ed.). Humana Press. https://books.google.com.sa/books?id=VWju7V4uIcgC

He, Y., Xu, P., Li, C., & Zhang, B. (**2005**). High-concentration food wastewater treatment by an anaerobic membrane bioreactor. *Water Research*, *39*(17), 4110–4118.

Helmer, R., Hespanhol, I., & WHO. (**1997**). *Water pollution control : a guide to the use of water quality management principles* (p. 56). London : E & FN Spon. https://apps.who.int/iris/handle/10665/41967

Herrera-Robledo, M., Cid-León, D. M., Morgan-Sagastume, J. M., & Noyola, A. (**2011**). Biofouling in an anaerobic membrane bioreactor treating municipal sewage. *Separation and Purification Technology*, *81*(1), 49–55.

Ho, J., & Sung, S. (**2009**). Anaerobic Membrane Bioreactor Treatment of Synthetic Municipal Wastewater at Ambient Temperature. *Water Environment Research*, *81*(9), 922–928.

Jain, M. (**2018**). Anaerobic Membrane Bioreactor as Highly Efficient and Reliable Technology for Wastewater Treatment—A Review. *Advances in Chemical Engineering and Science*, *08*(02), 82–100.

Koch, C., Fetzer, I., Schmidt, T., Harms, H., & Müller, S. (**2013**). Monitoring functions in managed microbial systems by cytometric bar coding. *Environmental Science and Technology*, *47*(3), 1753–1760.

Koch, C., Harnisch, F., Schröder, U., & Müller, S. (**2014**). Cytometric fingerprints: evaluation of new tools for analyzing microbial community dynamics. *Frontiers in Microbiology*, *5*(JUN), 273.

Korres, N., O'Kiely, P., Benzie, J. A. H., & West, J. S. (**2013**). *Bioenergy Production by Anaerobic Digestion: Using Agricultural Biomass and Organic Wastes* (Routledge (ed.)). Taylor & Francis. https://books.google.pt/books?id=0S2YAAAAQBAJ

Lam, P., & Kuypers, M. M. M. (**2011**). Microbial nitrogen cycling processes in oxygen minimum zones. *Annual Review of Marine Science*, *3*(1), 317–345.

Lambrecht, J., Cichocki, N., Hübschmann, T., Koch, C., Harms, H., & Müller, S. (**2017**). Flow cytometric quantification, sorting and sequencing of methanogenic archaea based on F420 autofluorescence. *Microbial Cell Factories*, *16*(1).

Lambrecht, J., Schattenberg, F., Harms, H., & Mueller, S. (**2018**). Characterizing microbiome dynamics – flow cytometry based workflows from pure cultures to natural communities. *Journal of Visualized Experiments*, *2018*(137), 1–16.

Li, P., Wang, Y., Wang, Y., Liu, K., & Tong, L. (**2010**). Bacterial community structure and diversity during establishment of an anaerobic bioreactor to treat swine wastewater. *Water Science and Technology*, *61*(1), 243–252.

Liao, B. Q., Kraemer, J. T., & Bagley, D. M. (**2006**). Anaerobic membrane bioreactors: Applications and research directions. *Critical Reviews in Environmental Science and Technology*, *36*(6), 489–530.

Lier, J. B. van, Mahmoud, N. A., & Zeeman, G. (**2008**). Anaerobic Wastewater Treatment. In M. Henze, M. van Loosdrecht, G. A. Ekama, & D. Brdjanovic (Eds.), *Biological Wastewater Treatment: Principles, Modelling and Design* (pp. 415–457). IWA Publishing. https://research.wur.nl/en/publications/anaerobic-wastewater-treatment

Martinez-Sosa, D., Helmreich, B., Netter, T., Paris, S., Bischof, F., & Horn, H. (**2011**). Anaerobic submerged membrane bioreactor (AnSMBR) for municipal wastewater treatment under mesophilic and psychrophilic temperature conditions. *Bioresource Technology*, *102*(22), 10377–10385.

Merlin Christy, P., Gopinath, L. R., & Divya, D. (**2014**). A review on anaerobic decomposition and enhancement of biogas production through enzymes and microorganisms. In *Renewable and Sustainable Energy Reviews* (Vol. 34, pp. 167–173). Elsevier Ltd.

Muhaidat, R., Al-Qudah, K., Al-Taani, A. A., & AlJammal, S. (**2019**). Assessment of nitrate and nitrite levels in treated wastewater, soil, and vegetable crops at the upper reach of Zarqa River in Jordan. *Environmental Monitoring and Assessment*, *191*(3).

Nopens, I., Capalozza, C., & Vanrolleghem, P. A. (**2001**). *Stability analysis of a synthetic municipal wastewater*. http://biomath.rug.ac.be

Perera, I. A., Abinandan, S., Subashchandrabose, S. R., Venkateswarlu, K., Naidu, R., & Megharaj, M. (**2019**). Advances in the technologies for studying consortia of bacteria and cyanobacteria/microalgae in wastewaters. *Critical Reviews in Biotechnology*, *39*(5), 709–731.

Proctor, C. R., Besmer, M. D., Langenegger, T., Beck, K., Walser, J. C., Ackermann, M., Bürgmann, H., & Hammes, F. (**2018**). Phylogenetic clustering of small low nucleic acid-content bacteria across diverse freshwater ecosystems. *ISME Journal*, *12*(5), 1344–1359.

Regueiro, L., Veiga, P., Figueroa, M., Alonso-Gutierrez, J., Stams, A. J. M., Lema, J. M., & Carballa, M. (**2012**). Relationship between microbial activity and microbial community structure in six full-scale anaerobic digesters. *Microbiological Research*, *167*(10), 581–589.

Ross, W. R., Barnard, J. P., Strohwald, N. K. H., Grobler, C. J., & Sanetra, J. (**1992**). Practical Application of the ADUF Process to the Full-Scale Treatment of a Maize-Processing Effluent. *Water Science and Technology*, *25*(10), 27–39.

Safford, H. R., & Bischel, H. N. (**2019**). Flow cytometry applications in water treatment, distribution, and reuse: A review. In *Water Research* (Vol. 151, pp. 110–133). Elsevier Ltd.

Scintillon Institute. (n.d.). *Spectral flow cytometry*. Retrieved September 22, 2020, from http://nolanlab.com/spectral-fc.html

Shin, C., & Bae, J. (**2018**). Current status of the pilot-scale anaerobic membrane bioreactor treatments of domestic wastewaters: A critical review. *Bioresource Technology*, *247*(August 2017), 1038–1046.

Sikosana, M. L., Sikhwivhilu, K., Moutloali, R., & Madyira, D. M. (**2019**). Municipal wastewater treatment technologies: A review. *Procedia Manufacturing*, *35*, 1018–1024.

Singh, K. S., & Viraraghavan, T. (**2003**). Impact of temperature on performance, microbiological, and hydrodynamic aspects of UASB reactors treating municipal wastewater. *Water Science and Technology*, *48*(6), 211–217.

Vincent, N. M., Wei, Y., Zhang, J., Yu, D., & Tong, J. (**2018**). Characterization and dynamic shift of microbial communities during start-up, overloading and steady-state in an anaerobic membrane bioreactor. *International Journal of Environmental Research and Public Health*, *15*(7), 1–20.

Wang, Y., Hammes, F., Boon, N., Chami, M., & Egli, T. (**2009**). Isolation and characterization of low nucleic acid (LNA)-content bacteria. *ISME Journal*, *3*(8), 889–902.

Wang, Y., Hammes, F., De Roy, K., Verstraete, W., & Boon, N. (**2010**). Past, present and future applications of flow cytometry in aquatic microbiology. *Trends in Biotechnology*, *28*(8), 416–424.

Win, T. T., Kim, H., Cho, K., Song, K. G., & Park, J. (**2016**). Monitoring the microbial community shift throughout the shock changes of hydraulic retention time in an anaerobic moving bed membrane bioreactor. *Bioresource Technology*, *202*, 125–132.

Zhang, Y., & Liu, W. T. (**2019**). The application of molecular tools to study the drinking water microbiome–Current understanding and future needs. *Critical Reviews in Environmental Science and Technology*, *49*(13), 1188–1235.

Appendix

Appendix A. Media and sampling frequency

Table A1. List of media components. The components have been grouped based on their main function.

Carbon source	
Starch	238.1 $mg.L^{-1}$
Na-acetate.3H_2O	256.9 $mg.L^{-1}$
Skimmed milk powder	226.7 $mg.L^{-1}$
Nitrogen source	
Yeast extract	101.9 $mg.L^{-1}$
Peptone	33.97 $mg.L^{-1}$
Nutrients and Iron	
$MgHPO_4.3H_2O$	56.62 $mg.L^{-1}$
KH_2PO_4	45.66 $mg.L^{-1}$
$FeSO_4.7H_2O$	11.32 $mg.L^{-1}$
Trace metals	
$Cr(NO_3)_3.9H_2O$	1.5 $mg.L^{-1}$
$CuCl_2.2H_2O$	1.05 $mg.L^{-1}$
$MnSO_4.H_2O$	0.21 $mg.L^{-1}$
$NiSO_4.6H_2O$	0.66 $mg.L^{-1}$
$PbCl_2$	0.2 $mg.L^{-1}$
$ZnCl_2$	0.41 $mg.L^{-1}$

Table A2. Influent stream expressed in water quality parameters (ammonia, nitrite, nitrate, phosphate, COD).

Influent water quality parameters	
Ammonia	37.5 $mg.L^{-1}$
Nitrite	0.074 $mg.L^{-1}$
Nitrate	0.133 $mg.L^{-1}$
Phosphate	123 $mg.L^{-1}$
COD	1247±77 $mg.L^{-1}$

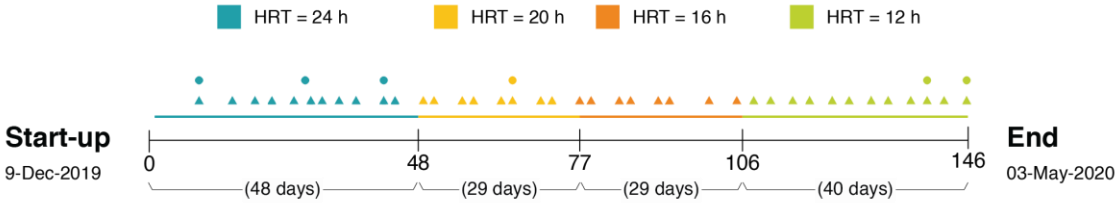

Figure A1. Sampling frequencies for which results have been analysed for biogas (continuous line), for liquid samples from the sludge tank bulk (triangles) and from the sludge tank but only for attached biomass (circles).

Appendix B. Flow cytograms

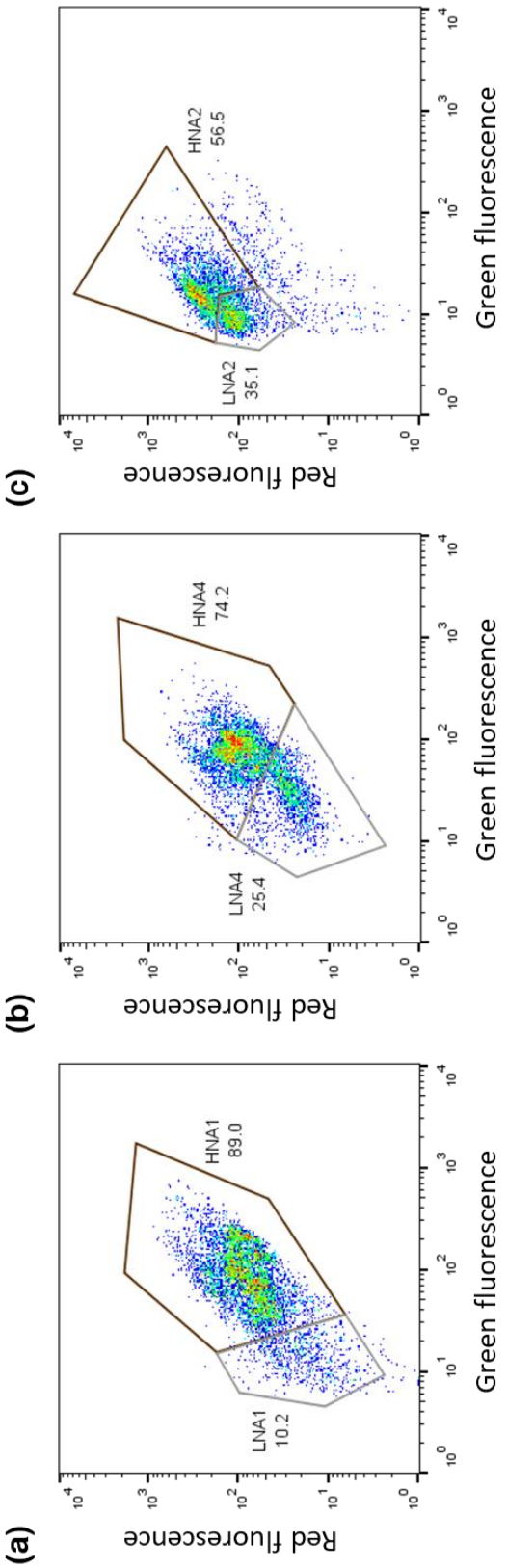

Figure B1. Gating strategy applied for quantification in HNA and LNA populations, respectively in the brown and grey polygonal gates, (a) days 0-124, except day 15, (b) day 15, (c) days 125-146. Cells were selected based on their green fluorescence as explained in the Methods' section and spread the red fluorescence axis to allow HNA and LNA quantification

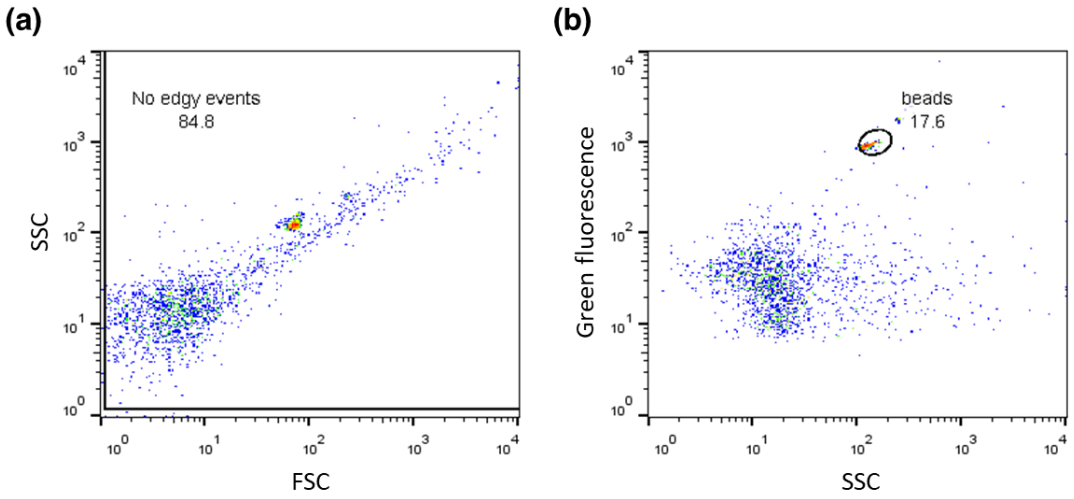

Figure B2. Gating strategy applied for quantification of cell events from effluent samples, (a) removal of all events on the edges in a forward and side scatters flow cytogram, FSC and SSC, respectively, (b) quantification of total cells based on the green fluorescence signal from nucleic acid stain and selection of the bead's population to later subtract to the former.

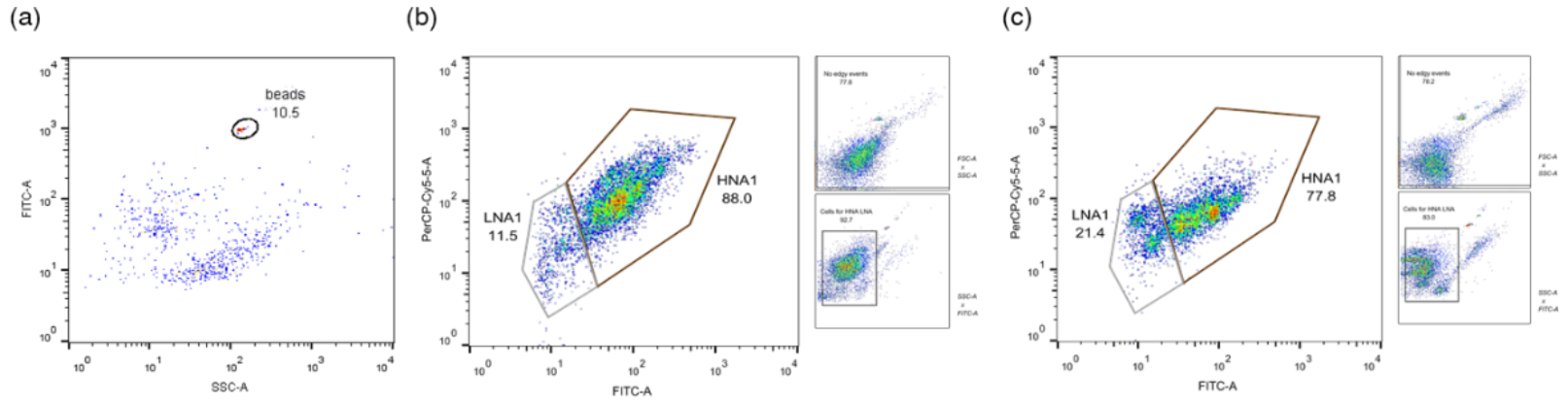

Figure B3. Flow cytograms representative of the beginning time point (day 9), (a) effluent, (b) sludge, (c) biomass. The smaller plots from (b) and (c) represent the backgating process (Methods) FSC vs SSC (top plot) and SSC vs FITC (down plot). The values near the polygonal gates represent the relative abundance of the events inside the gate from the total number of events.

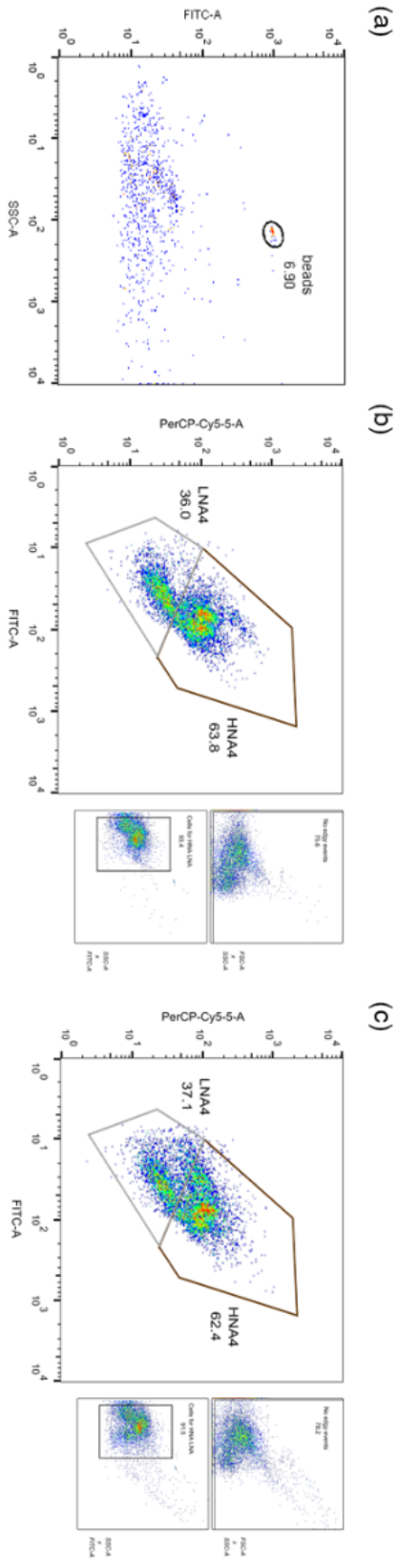

Figure B4. Flow cytograms representative of the end time point (day 146), (a) effluent, (b) sludge, (c) biomass. The smaller plots from (b) and (c) represent the backgating process (Methods) FSC vs SSC (top plot) and SSC vs FITC (down plot). The values near the polygonal gates represent the relative abundance of the events inside the gate from the total number of events.

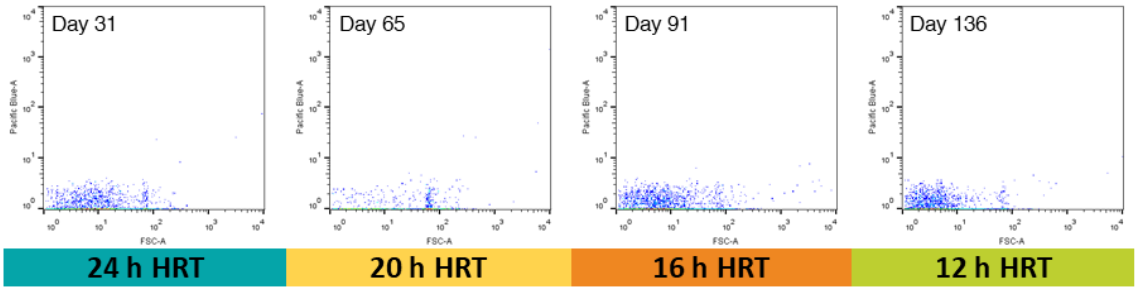

Figure B5. Flow cytograms representative of each of the studied HRTs (24 h, 20 h, 16 h and 12 h) for unstained samples.

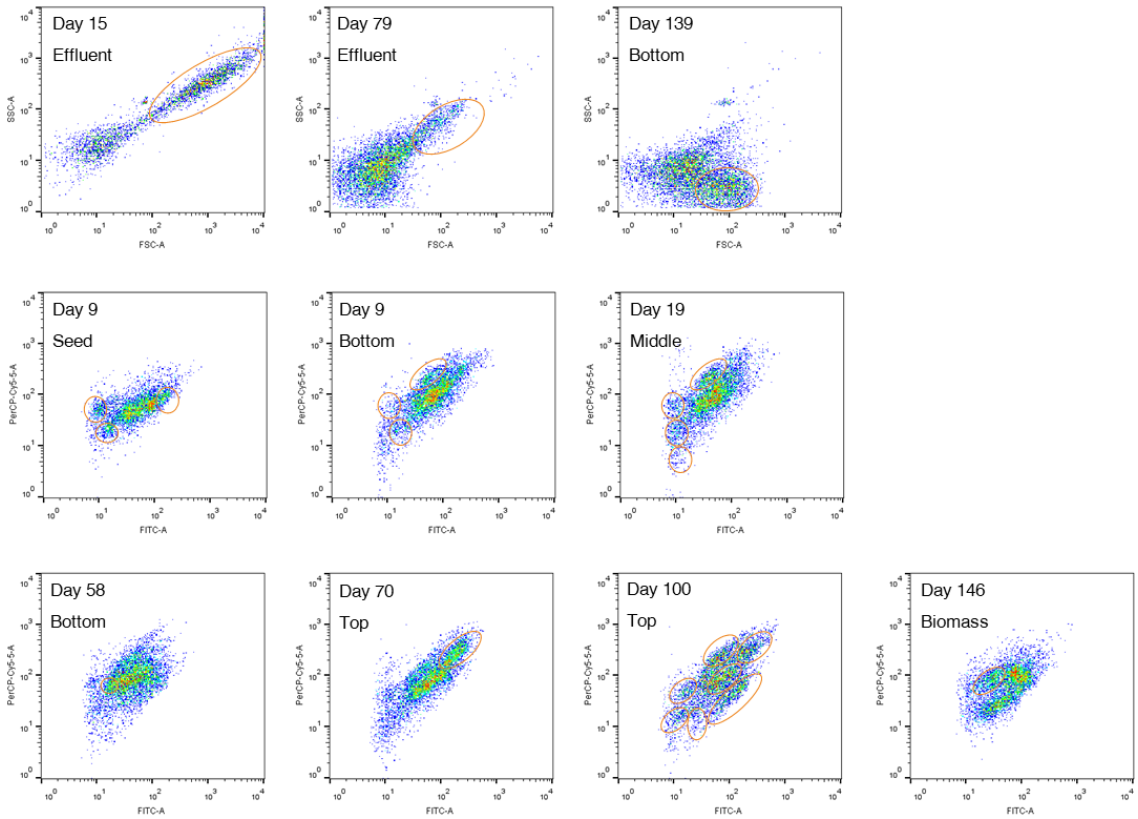

Figure B6. Flow cytograms with highlighted interesting subpopulations (orange ellipsis). The values near the elliptical gates represent the relative abundance of the events inside the gate from the total number of events.

Appendix C. Raw data

Table C1. Percentage of methane dissolved in sludge tank, membrane tank and effluent. At day 77 of the experiment the HRT has been changed from 20 h to 16 h.

Day	$\%_{CH_4 sludge\ tank\ dissolved}$	$\%_{CH_4 membrane\ tank\ dissolved}$	$\%_{CH_4 effluent\ dissolved}$
55	1.93	0.00	0.00
61	1.99	0.43	0.10
68	1.49	0.17	0.03
75	2.09	1.83	1.65
82	2.07	2.27	1.86
90	2.09	2.24	1.90
97	2.12	2.29	2.10

Table C2. COD fed and effluent values for different periods of time.

PERIOD OF DAYS	***COD_{feed} ($mg.L^{-1}$)***	***$COD_{effluent}$ ($mg.L^{-1}$)***
1 : 2	1119	480
2 : 8	1119	480
8 : 12	1119	480
12 : 18	1150	260
18 : 23	1200	137
26 : 33	1250	120
33 : 40	1250	138
40 : 47	1200	107
47 : 55	1150	113
55 : 61	1250	110
61 : 68	1300	110
68 : 75	1250	23
75 : 82	1300	16.5
82 : 90	1400	20
90 : 97	1330	15.5
97 : 104	1300	16
104 : 111	1300	16
111 : 118	1300	12
118 : 125	1250	5.2
125 : 132	1300	15
132 : 139	1300	12
139 : 146	1300	10.6

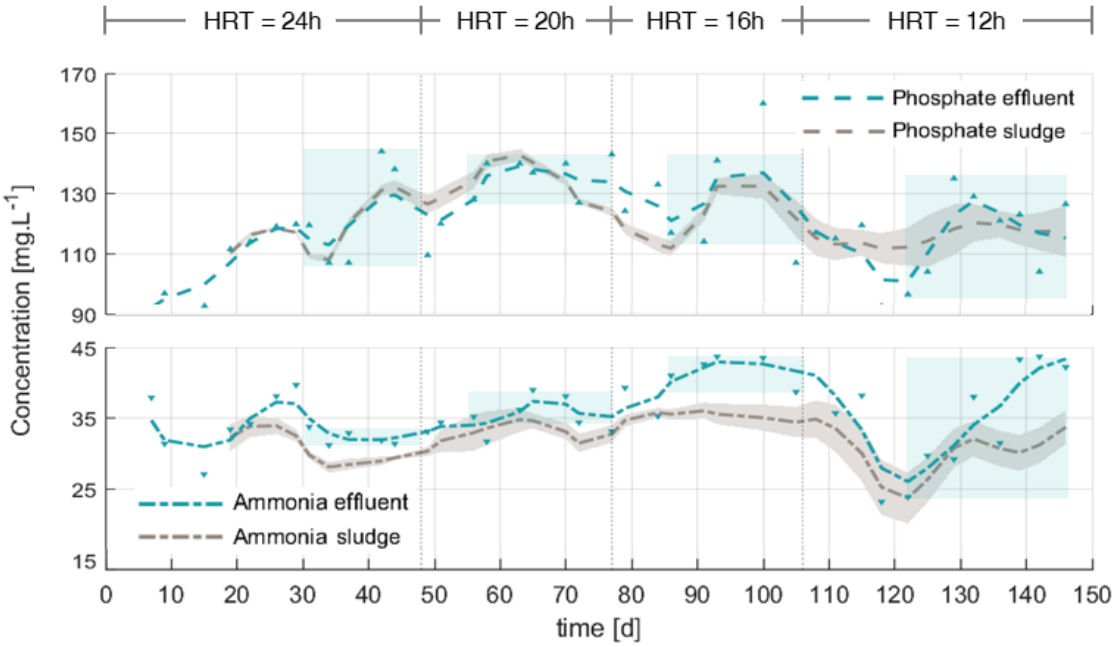

Figure C1. Phosphate and ammonia levels in sludge tank and effluent stream throughout the 146 days of operation of the pilot AnMBR. The trend lines are based on a moving average (n=3) filter applied to the results and the shaded irregular brown region demarks the standard deviation of the sludge measurements. The shaded rectangles represent the variation within the Y-axis on the considered stable domains of the effluent.

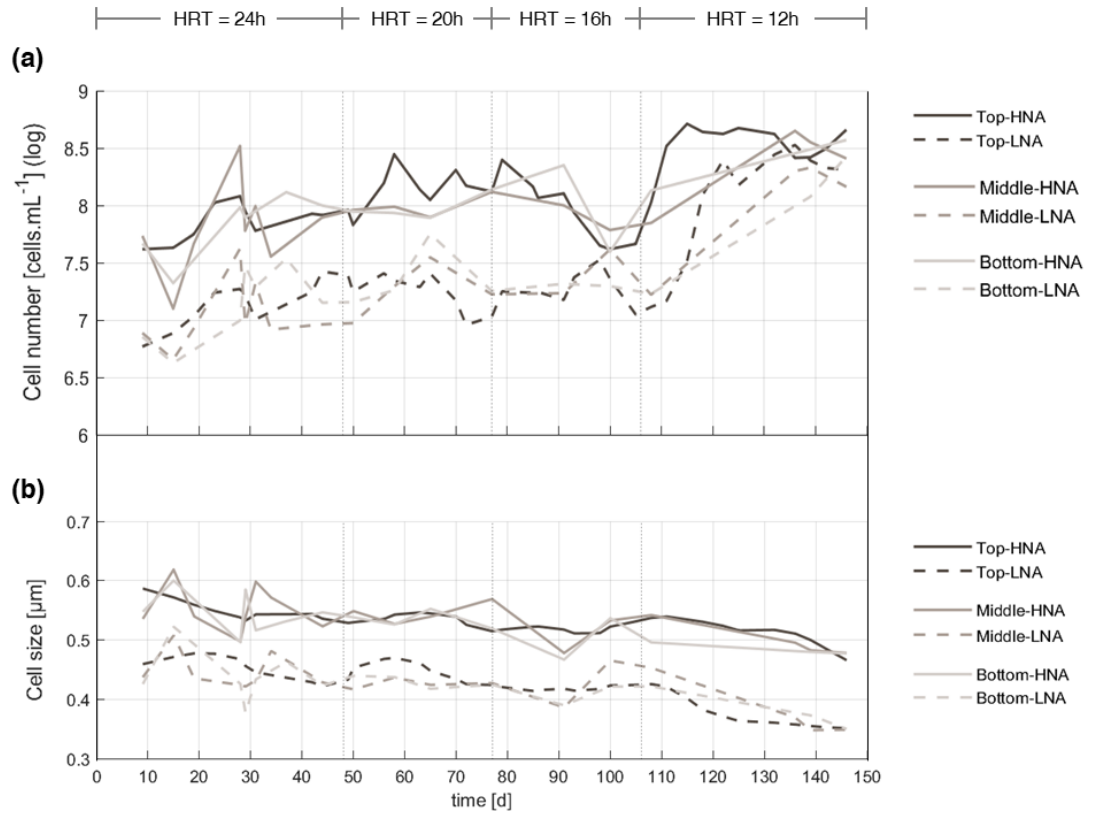

Figure C2. Samples from the top, middle and bottom of the sludge tank, (a) cell numbers per mL of sample, (b) median cell size.

Appendix D. HACH® kits

Table D1. HACH® test kits for either low or high range, depending on the concentration to be measured. These kits have been used for digesting the samples for means of water quality parameters (ammonia, phosphate, nitrate, nitrate and COD) assessment.

	LOW RANGE	***HIGH RANGE***
Ammonia	NA	Salicylate method 10031 (0-50 $mg.L^{-1}$)
Phosphate	NA	TNT 844 (1.5-15.0 $mg.L^{-1}$)
Nitrite	LCK 341 (0.015-0.6 $mg.L^{-1}$)	NA
Nitrate	LCK 339 (0.23-13.50 $mg.L^{-1}$)	NA
COD	LCK 314 (15–150 $mg.L^{-1}$)	LCK 514 COD (100–2000 $mg.L^{-1}$)